STELLAR POPULATIONS AND VELOCITY DISPERSIONS OF TEN NEARBY GALAXIES

Thesis by

Theodore Burton Williams

In Partial Fulfillment of the Requirements

for the Degree of

Doctor of Philosophy

California Institute of Technology

Pasadena, California

1976

(Submitted October 20, 1975)

To the Memory of

Dennis Palm

ACKNOWLEDGEMENTS

The completion of this thesis depended upon the interest and support of many people, to whom I cannot adequately express my gratitude. In particular, I wish to thank:

Janet, for her affection in the face of the pomposity of science and its practitioners;

Jesse Greenstein, for his advice, from the inception to the completion of this project;

Drs. Jim Gunn, Barry Turnrose, and Francois Schweitzer, for providing data in advance of publication;

Ed Turner for his algorithms, advice, and friendship (in inverse order of importance);

Larry Blakee, Martin Olsiewski, Bud Smith, Bob Cadman, and Leroy Kimoto for keeping recalcitrant electronics functioning just long enough;

Richard Green and John Huchra, for their camaraderie;

Drs. Maarten Schmidt and Jim Gunn, for proving that great scientists can be great people;

John Hoessel for his assistance with many parts of this project;

The 60" night assistants, Chip Williams, Brad Bailey, and Steve Barry, for struggling with overwhelming

numbers of bright stars;

Helen Holloway, Elsa-Brita Titchenell, and Janet Williams, for typing the manuscripts of these papers;

The graduate students and faculty of the astronomy department, for their advice and assistance;

The National Science Foundation, for three years of support.

ABSTRACT

Previous attempts to synthesize the stellar populations of galaxies using unconstrained best fit algorithms yield astrophysically unreasonable models. Numerical experiments are performed which indicate that this behavior is due to noise in the data. Best fit models, constrained or not, are insensitive to the actual galaxy stellar population.

Spectra from 3800 Å to 6800 Å with resolution of 2 Å have been obtained for 137 stars, 5 globular clusters, and the nuclear regions of 10 galaxies. Line indices measured for 74 absorption lines and bands are presented. A method for determining parametrized stellar population models is discussed, and is shown to be stable in the presence of noise. Population models and error estimates are derived for the ten galaxies. Most of the models have significant contributions from M giant stars and from metal poor stars. Only two of the galaxies seem to contain stars with metal lines stronger than those of stars in the solar neighborhood. Three of the ellipticals show evidence of recent star formation, possibly due to infall of gas from nearby spirals. The galaxies studied here can be divided by morphological type into three distinct population groups: E0 - Sa, Sb, and Sc.

Velocity dispersions have been derived for the nuclear regions of the galaxies. These dispersions are estimated by comparing broadened composite stellar spectra with the galaxy spectra. The composite spectra give systematically lower velocity dispersions than those estimated from fitting with single stars. Mass to light ratios are derived from the velocity dispersions. These mass to light ratios are low, and there are no systematic differences between the nuclei of spirals and ellipticals.

TABLE OF CONTENTS

INTRODUCTION

This thesis consists of the manuscripts of three papers submitted to the Astrophysical Journal. Each of these papers is intended to be read independently of the others, and thus is unavoidably somewhat redundant. The references for each paper are presented at the end of each chapter, not collected into a single reference section at the end of the thesis. I apologize in advance for any difficulties that these discontinuities may cause, and hope they do not disrupt the essential unity of these investigations.

The first chapter is a criticism of previous analytic methods of population synthesis, and provides the motivation for the method used in this study. The second chapter describes the observations and data reduction procedure. It presents a method of population synthesis superior to those discussed in the first chapter, and uses it to deduce the populations of the galaxies studied. It also contains in tabular form all of the measurements of the star and galaxy spectra. The last chapter uses the population models of the second chapter to construct synthetic spectra, which are broadened to estimate the velocity dispersions of the galaxies.

CHAPTER 1

THE EFFECTS OF NOISE ON GALAXY POPULATION SYNTHESIS

In recent years, several authors have attempted to deduce the stellar composition of galaxies from their composite light, as measured by photometric scanners with resolutions on the order of 20 Å, or by spectrographs with typical resolutions of 2 Å. Faber (1972), followed by Jolly (1974) and Turnrose (1975) have used various mathematical techniques to find that mix of stars, subject to various astrophysical constraints, which reproduces the observed galaxy light with smallest residual differences. Numerical experiments described below indicate that such best fit models are determined by the noise in the data, and are insensitive to the actual galaxy stellar population.

A detailed discussion of my own observational procedures and reduction techniques will appear in a subsequent paper (Williams 1976). Briefly, the Palomar 1.5 m telescope equipped with a two-stage image-tube spectrograph was used to obtain spectra of 10 galaxies, 137 stars, and 5 globular clusters. The spectra extend from 3800 Å to 6800 Å, at a dispersion of 50 Å mm^{-1}, with resolution of 2 Å. The spectra are measured with a digital microphotometer, corrected for the nonlinear film response, shifted to zero velocity, and corrected for the geometric distortions of the image tube. Comparison of the reduced spectra with scans of standard stars obtained by Dr. J. E. Gunn using the multichannel spectrophotometer on the 5 m telescope indicates

total errors no greater than 5% in the spectroscopic data.

Line indices are measured for 74 absorption lines and bands arising from various elements and levels of excitation. These indices are defined as the ratio of the relative intensity in a band centered on the feature to the relative intensity in a band centered several angstroms away. The bands are broad enough so that the indices are independent of the velocity dispersion in the galaxy. The spacing between the feature band and the side band is small enough so that the energy distribution of the galaxy, interstellar reddening, and atmospheric extinction do not affect the indices. Since the indices are defined without reference to an artificial continuum, they are inherently much more accurate than equivalent width measurements for late type stars.

A computer algorithm has been devised which computes the composite line indices for a mix of stellar types, evaluates the residual difference between computed and observed galaxy line indices, and changes the mix of stars to reduce this residual. This procedure is iterated until the model converges to a minimum residual. Starting from many different initial models, the algorithm consistently converges to the same best fit model for a given galaxy. This indicates that for each galaxy discussed below, there is probably only one minimum in the range of acceptable solutions.

The first models of the nucleus of M31 were constrained to allow only nonnegative numbers of each type of star. One such model is shown in Figure 1. The model is implausible. Huge gaps exist along the main sequence, subgiant and giant branches, which are expected to be smooth and continuous. Furthermore, if negative numbers of stars were allowed, the groups at the bottom of the plot would go strongly negative. Other authors, using data of different resolution, covering different spectral ranges, and using different modeling algorithms, have observed exactly the same behavior. Their response has been to require plausible models by imposing astrophysical constraints on the modeling algorithms (e.g. Faber 1972). Typical constraints require continuous sequences, with slopes and relative populations compatible with observed cluster populations and stellar evolution theory.

Before imposing such constraints, a series of numerical experiments has been performed to investigate the non-physical nature of the unconstrained models. Any given number distribution of stars defines a pseudo-galaxy; the composite line indices of this pseudo-galaxy are the flux weighted sums of the stellar line indices. One such pseudo-galaxy, similar to Faber's (1972) basic model for M31, is shown as the solid curve in Figure 2. A best fit model for this pseudo-galaxy is computed, with the result illustrated

FIGURE 1

The unconstrained model for the nucleus of M31. The logarithm of the relative number of stars used is shown for each star group. Points at the bottom boundary of the figure represent $N \leq 10^{10}$. The crosses are normal abundance stars, the circles super metal rich stars. HB refers to horizontal branch stars, GC to globular clusters (metal content increases to right), and PII to Population II giants. There are large gaps between stars of similar type along the sequences.

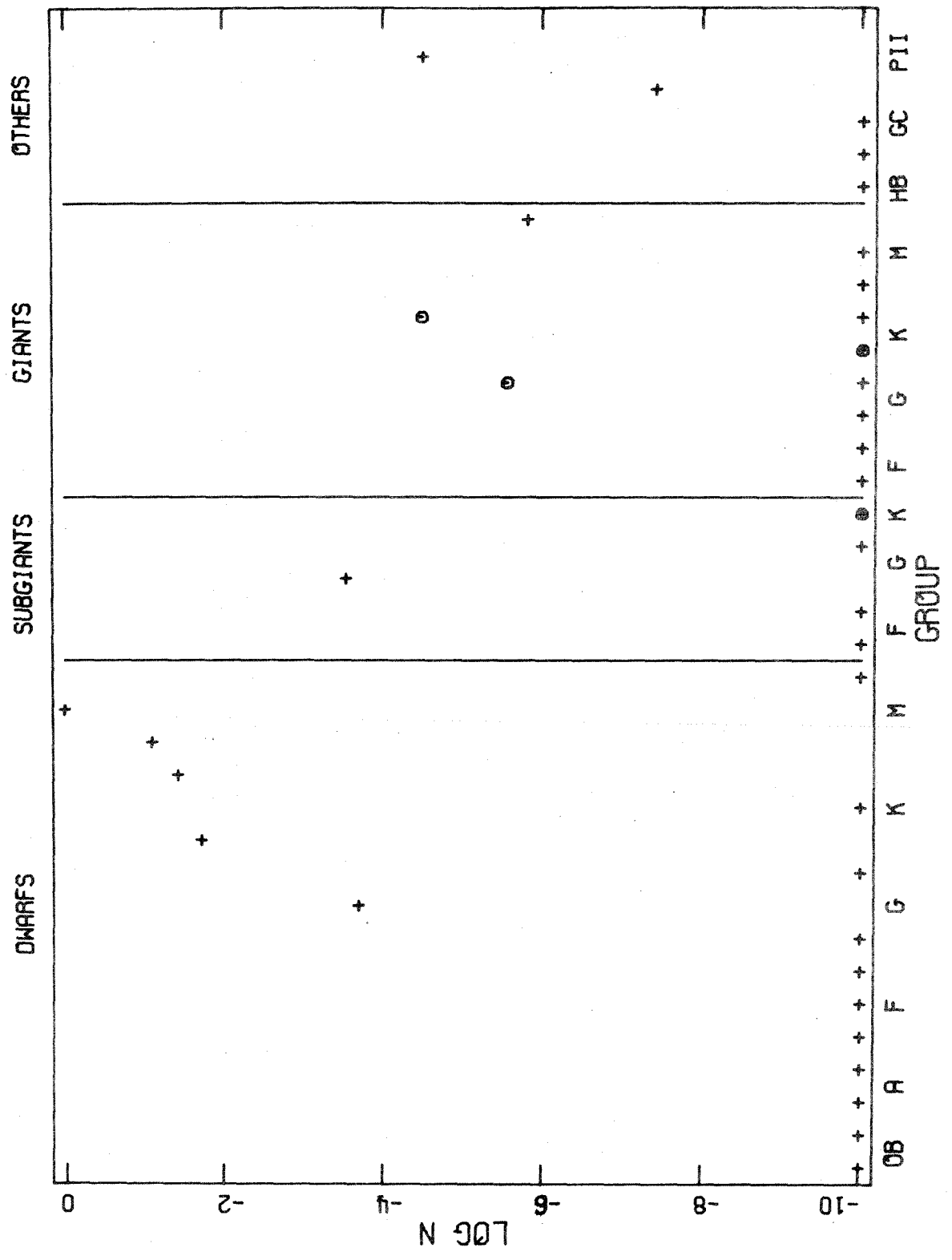
DWARFS
SUBGIANTS
GIANTS
OTHERS
OB A F G K M F G K M HB GC PII
GROUP
0 -2 -4 -6 -8 -10
LOG N

by the points in Figure 2. These best-fit models are smooth and continuous, and are very good reproductions of the pseudo-galaxy. This particular model does not discriminate between late F dwarfs, subgiants, and giants. The only discrepant points are early A dwarfs and Population II giants, both of which contribute negligible amounts of light. The pseudo-galaxy is then perturbed with randomly distributed 5% noise and again modeled. The arrows in Figure 2 show the change in the model induced by the noise. All of the inconsistencies of the unconstrained models of real galaxies are present here. Similar behavior is found in several other cases of different pseudo-galaxies perturbed with different random noise distributions. Thus it is clear that small amounts of noise in the data are sufficient to produce the unacceptable nature of unconstrained best fit models observed in this work and by other authors.

A limited investigation of pseudo-galaxies perturbed by 1% random noise suggests that the same instabilities are present in best fit models of data of higher accuracy. This tentative conclusion is supported by the fact that the unconstrained best fit models of Faber (1972) and Turnrose (1975), constructed from high accuracy photoelectric data, suffer all of the difficulties outlined above. Moreover, if the library of stars available for synthesis does not include all of the types of stars actually present in the

FIGURE 2

The effect of small amounts of random noise. The solid curve is the pseudo-galaxy; the points are the best-fit model. The arrows show the change in the model due to 5% noise perturbations of the pseudo-galaxy. The best-fit model is normalized to the curve at the early K giants.

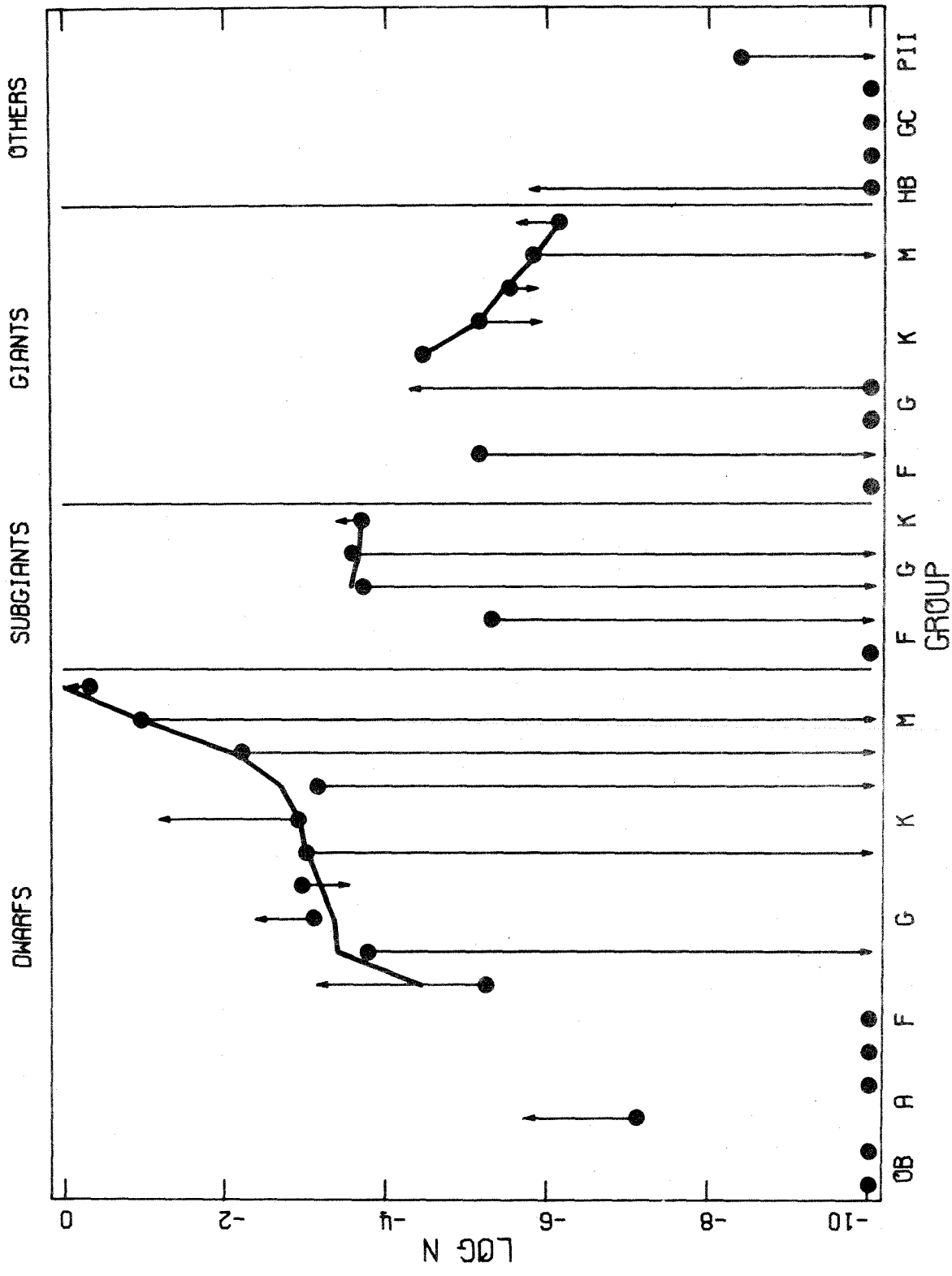
DWARFS
SUBGIANTS
GIANTS
OTHERS
OB A F G K M F G K M K G F M HB GC PII
GROUP
LOG N
0
-2
-4
-6
-8
-10

galaxy, the best fit models are similarly unstable. Such a deficiency occurs if, for example, the nucleus of a galaxy is more metal rich than any star in the solar neighborhood (cf. M31 model by Spinrad and Taylor 1971). It thus appears that much higher accuracy will not solve the problems encountered above.

Since unconstrained best fit models are determined almost entirely by the noise, they are very insensitive to the actual stellar population of the galaxy. Furthermore, applying such constraints as mentioned above does not make the method more sensitive to the stellar population. These constraints allow only a subset of all the possible models to be considered; the best fit algorithm then picks from this subset that member which has the smallest residual differences from the observed galaxy. Such a model is either that member of the subset which is nearest to the unacceptable unconstrained minimum, or a member at a secondary minimum in the allowed region. The former case merely returns the values of the constraints used. There is no reason to believe that the secondary minimum of the latter case contains any more information about the actual population than the unallowable primary minimum. Indeed, in the numerical experiments described above, pseudo-galaxies perturbed with noise possessed no secondary minima near the actual stellar distribution. Thus best fit models, constrained or not,

contain little information about the actual stellar population.

The proper method of stellar population synthesis is to restrict the number of degrees of freedom available to the models until they lose their sensitivity to noise. The range of such models which fit the data must then be systematically explored. Such a method does not merely produce results primarily determined by noise and the constraints imposed, but actually extracts information about the galaxy from the data. A method of parameterized models will be presented in a subsequent paper (Williams 1976) which attempts to realize these goals.

The author would like to thank Ed Turner for his helpful discussions during the course of this work, and Dr. J. E. Gunn for kindly providing data in advance of publication. The author was supported during part of this work by a National Science Foundation pre-doctoral fellowship.

REFERENCES

Faber, S. M. 1972, Astr. and Ap., 20, 361.

Jolly, M. 1974, Astr. and Ap., 33, 177.

Spinrad, H., and Taylor, B. 1971, Ap. J. Suppl., 22, 445.

Turnrose, B. E. 1975, Ph.D. Thesis, California Institute of Technology.

Williams, T. B. 1976 (in preparation).

CHAPTER 2

POPULATION SYNTHESIS OF THE NUCLEI OF TEN NEARBY GALAXIES

I. INTRODUCTION

One of the first attempts to deduce the stellar populations of galaxies from the spectrum of their composite light was performed by Morgan and Mayall (1957), who visually compared photographic spectra of galaxies with those of stars. Subsequent investigations were based upon photoelectric photometry with resolution on the order of 20 Å . Such observations have been performed most recently by Spinrad and Taylor (1971) and by Turnrose (1975). Jolly and Andrillat (1973) have attempted to obtain high resolution data for M31 using photographic spectra. Along with the improvements in observational data, several authors have attempted to improve the methods of analysis of those data. Spinrad and Taylor applied astrophysical constraints in a trial-and-error process to guess an adequate representation of the data. Faber (1972), Jolly (1974), and Turnrose (1975) have used various analytic methods to produce the best fits to the observations; Williams (1976) has shown that these attempts were highly influenced by noise in the data, however.

This investigation uses the high speed of an image-tube spectrograph to obtain high resolution data of sufficient photometric accuracy to perform population syntheses on the nuclei of ten nearby galaxies. A method of analysis is used which avoids the sensitivity to noise of the previous

investigations. The observations are presented in section II, the photometric calibration procedure in section III, and the data reduction methods in section IV. Section V discusses the synthesis procedure. Results are presented for the individual galaxies in section VI, and for the ten galaxies as a whole in section VII. Finally, section VIII presents conclusions about these results and recommendations for future work.

II. OBSERVATIONS

The observations for this project were made between 1974 January and 1975 April, using the Palomar 1.5-meter telescope equipped with the Cassegrain two-stage image-tube spectrograph. Three spectra were required to cover the wavelength range from 3800 Å to 6800 Å; these spectra are described in Table 1. Care was taken to reproduce the instrument settings exactly at each observing session, to minimize systematic differences between the spectra. Thus, for example, the variation of sensitivity over the face of the image-tube photocathode did not systematically affect the measurements, since any given wavelength always fell on the same physical spot on the photocathode. The spectra were recorded on unbaked IIa-D film.

Spectra were obtained for 137 stars and 5 globular clusters. The stars cover the main sequence from late O to

TABLE 1

DESCRIPTION OF SPECTROGRAMS

Wavelength Range (Å)	Nominal Dispersion (Å mm^{-1})	Slit Width Projected on Sky (arc sec)	Slit Width Projected on Film (Å)
3700 - 4500	38	3.75	2.1
4200 - 5700	62	3.00	2.5
5500 - 6900	57	3.00	2.5

late M, the subgiant branch from early F to early K, and the giant branch from early F to late M. For the K giants and subgiants there are two complete sequences, one of stars with normal metal abundances, and one of stars termed "super metal rich". The globular clusters, horizontal branch stars and population II giants represent a metal poor population. The stars, which all have published spectral types and luminosity classes, were selected to have apparent visual magnitudes of approximately 8, whenever possible, so that the exposure times would be on the order of one minute. The stars were selected from the following sources: Moore and Paddock (1950), Gliese (1969), Veeder (1974), Jaschek (1964), Spinrad and Taylor (1971), and Faber (1972). The stars are listed by group in Table 2. The masses and luminosities in Table 2 are compiled from Blaauw (1973), Vyssotsky (1963), Keenan (1963), Blaauw (1963), Harris, Strand and Worley (1963), Spinrad and Taylor (1971), and Faber (1972). Fluxes over this wavelength range for star groups similar to these are tabulated in Turnrose (1975), O'Connell (1970), and Christensen (1972). The ratio of the flux at 3800 Å to the flux at 6800 Å varies from 2.83 for the OB dwarfs, through 0.27 for G dwarfs to 0.04 for M dwarfs. The spectra for all stars were widened to 0.3 mm by an oscillating quartz block located behind the slit of the spectrograph. For the globular clusters, the slit length was set to the apparent

TABLE 2

STAR GROUPS

Group Name	Mass ($M_\odot$)	V Light ($L_\odot$)	Parametric Variable	Group Members*			
OB V	10.0	2.8E+3	10.0	93521	160186	185418	-8°4617
late B V	3.0	8.3E+1	3.0	30650	106420	110166	182489
early A V	2.0	2.5E+1	2.0	32418	109268	109615	190785
late A V	1.7	1.1E+1	1.7	73430	99473	109068	+29°3811
early F V	1.4	5.3E+0	1.4	30247	113036	126516	157683
mid F V	1.3	2.8E+0	1.3	25322	105679	168621	173189
late F V	1.2	1.9E+0	1.2	22872	120893	147644	175036
early G V	1.0	1.0E+0	1.0	56274	107582	110950	210483
mid G V	0.95	5.3E-1	0.95	12783	44420	174719	192343
late G V	0.90	3.0E-1	0.90	64606	144287	156826	220140
early K V	0.70	1.7E-1	0.70	73667	125455	177830	211472
mid K V	0.65	4.0E-2	0.65	GL301.1	139323	154363	217580
late K V	0.60	1.6E-2	0.60	GL397	86586	110315	202575
early M V	0.40	6.9E-3	0.40	1326	GL424	95735	131976	193202
mid M V	0.20	1.3E-3	0.20	GL251	GL273	GL699	119850	239960
late M V	0.15	1.2E-4	0.15		GL15B	GL83.1	GL234	
early F IV	1.2	1.1E+1	1.93	11012	88513	156536	210891
late F IV	1.2	6.3E+0	1.39	5072	26596	27816	103628
early G IV	1.2	4.0E+0	1.00	11170	74811	84606	140514
late G IV	1.2	2.8E+0	0.72	502	53590	77391	81265
early K IV	1.2	2.5E+0	0.52	44019	157072	192260	197206
early K IV SMR	1.2	2.5E+0	0.52		HR258	HR495	HR5227	
early F III	2.0	2.8E+1	1.93	1552	12637	96294	157925
late F III	2.0	2.8E+1	1.39	16314	17055	60983	179985
early G III	2.0	3.0E+1	1.00	48688	122052	134063	191737
late G III	2.0	3.6E+1	0.72	31324	117125	129391	211645

TABLE 2 — continued

Group Name	Mass ($M_\odot$)	V Light ($L_\odot$)	Parametric Variable	Group Members*			
late G III SMR	2.0	3.6E+1	0.72		HR3369		
early K III	2.0	4.8E+1	0.52	51228	110194	128200	210922
early K III SMR	2.0	4.8E+1	0.52	HR1805	HR5582	HR7576	
late K III	2.0	1.0E+2	0.37	35146	93391	153540	157606
late K III SMR	2.0	1.0E+2	0.37		HR5826	HR6136	
early M III	1.5	1.4E+2	0.30	40931	113406	128684	183681
mid M III	1.5	1.9E+2	0.24	74225	153698	181312	210514
late M III	1.5	2.5E+2	0.19	11961	90068	203712	207076
horizontal br.	0.5	3.0E+1	1.0E-2	86986	109995	161817	
Population II	0.9	1.0E+2	1.0E-2	HR5270	2665	165195	221170
globular cl. I	1.0E+5	1.0E+5	1.0E-5		NGC6341	NGC7078	
globular cl. II	1.0E+5	1.0E+5	1.0E-5		NGC5272	NGC5904	
globular cl. VI	1.0E+5	1.0E+5	1.0E-5		NGC6356		

*No prefix: HD; GL: Gliese (1969)

diameter of the visible image of the part of the cluster not resolved into individual stars. The cluster light was integrated by moving the image of the cluster over the slit as the exposure was taken.

Spectra were obtained for the nuclear regions of ten galaxies. The galaxies were selected to cover the range of morphological types from E0 to Sc, to have high surface brightness in the nuclear region, and to have fairly sharp absorption lines. The galaxies observed are listed in Table 3. The magnitudes listed are from de Vaucouleurs (1964); the morphological types from Sandage (1961), and de Vaucouleurs (1964). Several spectra were obtained for each galaxy in each wavelength region as noted in Table 3. For all galaxy spectra the slit was oriented perpendicular to the major axis of the galaxy, was centered on the nucleus, and had a length of 15 arc sec projected on the sky. This slit length corresponds to 45 pc at the nearest galaxies, 1.5 kpc at the most distant. Thus the light observed comes from the nucleus and surrounding regions. The spectra were widened to 0.3 mm with the oscillating quartz block.

TABLE 3

GALAXIES OBSERVED

Galaxy (NGC)	Morphological Type	B Magnitude (mag.)	Number of Spectra Obtained		
			Blue	Green	Red
221 (M32)	EO	5.39	3	3	3
224 (M31)	Sb	4.61	3	3	3
584	E4	11.71	2	2	2
1052	E4	12.12	2	2	1
3031 (M81)	Sb	7.88	3	4	4
3115	SO	10.43	3	3	3
3379	E1	10.83	2	2	2
4473	E5	11.79	3	2	2
4594 (M104)	Sa	9.52	3	3	3
5194 (M51)	Sc	9.03	4	3	3

III. INTENSITY CALIBRATION

The spectra were calibrated by exposing one or more calibration wedges on the same strip of film. The wedge varied logarithmically over two orders of magnitude in intensity; the light source was filtered to resemble the color of the image tube phosphor. The exposure times of the wedges were comparable to those of the spectra. Since the wedges were on the same strip of film as the spectra, they received exactly the same chemical processing. The calibrations were applied by a separate calibrating device, not through the image tube.

The calibration wedges were reduced using a modified form of the method of opacitance discussed by de Vaucouleurs (1967). The opacitance, ω, is defined as

$$\omega(x) = \frac{C-D}{t(x)-D} - 1.0$$

where C is the clear plate transmission, D is the dark count, and t(x) is the transmission at any point x on the film. The advantage of the opacitance representation over a density representation is that log intensity is a smooth function of log ω over a wide range of ω, and is adequately fit by a polynomial expansion in log ω. A fifth order expansion was used for each wedge, with residuals of four percent or less.

To determine whether any systematic differences existed

between the wedge calibrations and calibrations through the spectrograph-image tube system, a series of spectra of an incandescent lamp filtered with calibrated neutral density filters was taken at the telescope. These spectra were exposed in exactly the same manner as the star and galaxy spectra, and a calibration wedge was applied to the film. The wedge and calibration spectra agreed to within 2 percent. We concluded that the wedges provide an adequate calibration of the image tube-spectrograph system.

IV. DATA REDUCTION

Because of the large number of spectra involved, and to maintain uniform treatment of each spectrum, an automated reduction procedure was adopted. The calibration exposures and spectra were scanned with a digital microphotometer and the resultant digitized transmission recorded on magnetic tape. The microphotometer slit was 20 by 300 microns, projected on the film; the digitization step size was 6 microns. Various tests of this microphotometer indicate an overall positional accuracy not worse than 4 microns.

A computer code was written to reduce the digitized data from the microphotometer. The first step of the procedure was to analyze the comparison spectra for each film. The comparison lines were found using an algorithm described in the appendix, and the lines were identified. The line wavelengths were fit by a third order polynomial of the

line position on the film; the error for an individual line in the fit was typically 0.4 Å or less. Next, all of the absorption and emission lines in the object spectrum were found. Using an algorithm provided by E. Turner (1976), these lines were identified and the velocity of the object determined. The error of these velocities was on the order of 30 km s^{-1}. The information from the appropriate calibration wedge was then used to convert the transmission data to relative intensities. The geometric distortions introduced by the image tube were removed, and the object was shifted to zero velocity with respect to the Earth. These linearized spectra had a sample size of 0.25 Å in the blue, and 0.33 Å in the green and red. This final digital image of relative intensity versus wavelength was written onto magnetic tape for further processing.

The accuracy of the reduction procedure described above was verified by comparison of the reduced spectra to scans of stars obtained by Dr. J. E. Gunn using the multichannel spectrophotometer on the 5-meter telescope. These scans were averaged into stellar groups by B. Turnrose, who kindly provided the data in advance of publication. The data from the image tube spectra were corrected for extinction and reddening, and summed over the bandpasses of the multichannel. The response of the image-tube system as a function of wavelength was determined by fitting with a low

order polynomial the ratio of the flux in the multichannel bands to that in the bands synthesized from the spectra. After this response function was removed from the spectra, they agreed with the multichannel data to within 5 percent. We thus conclude that the relative intensities determined by the image-tube spectra are accurate to 5 percent or better.

Line indices were measured for 74 absorption lines and bands. These indices measure 7 hydrogen lines, 5 helium lines, 14 molecular bands, 40 low excitation metal lines, and 7 high excitation metal lines. Included are lines sensitive to temperature and luminosity in the stars, as discussed by Gahm (1970), Gahm and Hultquist (1972), Strömgren (1963), Keenan (1963), and Morgan, et al. (1943). These indices are defined as the ratio of the relative intensity in a band centered on the feature to the relative intensity in a band centered several angstroms away. The bands are broad enough so that the indices are independent of the velocity dispersion in the galaxy. The spacing between the feature band and the side band is small enough so that the energy distribution in the object, interstellar reddening, and atmospheric extinction do not affect the indices. Since the indices are defined without reference to an artificial continuum, they are inherently much more accurate than equivalent width measurements for late type stars. The indices are described in Table 4. The values of the indices

TABLE 4

DESCRIPTION OF LINE INDICES

Band Number	Line Band Center (Å)	Line Band Width (Å)	Side Band Center* (Å)	Feature
1	3835	5	3848	H
2	3888	5	3895	H + He
3	3933	20	3910	CaII
4	3968	20	3990	H + CaII
5	4005	5	4010	Fe
6	4030	10	4020	He + Mn
7	4045	5	4050	Fe
8	4063	5	4055	Fe
9	4077	5	4085	SrII
10	4101	15	4115	H
11	4133	5	4125	Mn
12	4143	5	4150	He + Fe
13	4171	10	4180	Ti + CN
14	4200	10	4185	SiII
15	4215	5	4210	Fe + SrII + CN
16	4226	10	4235	Ca
17	4271	10	4280	Fe + Cr
18	4289	5	4280	Cr
19	4305	20	4318	G Band
20	4325	10	4330	Fe
21	4340	10	4330	H
22	4352	5	4348	Fe + Mg
23	4374	5	4370	Fe
24	4383	10	4390	Fe
25	4404	10	4395	Fe
26	4415	5	4420	Fe
27	4455	10	4445	Ca
28	4471	5	4465	He
29	4481	5	4490	MgII
30	4460	15	4450	Fe
31	4530	10	4520	Fe
32	4583	5	4590	TiO
33	4649	5	4635	Fe
34	4731	10	4740	Mg
35	4761	10	4750	TiO + MgH
36	4861	15	4845	H

TABLE 4 (CONT.)

DESCRIPTION OF LINE INDICES

Band Number	Line Band Center (Å)	Line Band Width (Å)	Side Band Center* (Å)	Feature
37	4920	5	4910	Fe
38	4960	10	4950	TiO
39	4982	10	4990	Ti
40	5015	10	5025	He
41	5041	5	5050	SiII
42	5082	5	5090	Fe
43	5112	5	5120	Ti + Fe
44	5170	10	5155	Mg + TiO
45	5183	10	5195	Mg
46	5208	5	5220	MgH
47	5229	5	5235	Fe
48	5270	10	5285	Ca
49	5300	5	5310	Fe + Ti
50	5330	10	5315	Fe
51	5371	10	5381	Fe
52	5410	10	5420	Fe
53	5455	10	5440	TiO
54	5711	5	5720	Mg
55	5765	5	5750	TiO
56	5784	5	5790	Ti
57	5815	5	5805	Ti
58	5855	5	5845	TiO
59	5892	10	5880	Na
60	5955	5	5950	Ti
61	5971	5	5980	YO
62	6135	5	6130	Fe + YO
63	6155	5	6150	TiO
64	6165	5	6175	TiO
65	6225	5	6230	TiO
66	6420	5	6410	Fe
67	6450	5	6460	Ca
68	6488	5	6480	...
69	6497	10	6510	Ba
70	6550	5	6540	...
71	6562	10	6570	H
72	6722	5	6715	Si
73	6747	10	6755	Fe
74	6787	5	6780	MgII

TABLE 4 (CONT.)

DESCRIPTION OF LINE INDICES

*All side band widths are 5 Å.

TABLE 5

LINE INDEX DATA

LINE	OB V	LATE B V	EARLY A V	LATE A V	EARLY F V	MID F V	LATE F V	EARLY G V	MID G V	LATE G V	EARLY K V	MID K V	LATE K V
1	0.769	0.472	0.356	0.437	0.498	0.532	0.565	0.538	0.709	0.595	0.625	0.694	0.704
2	0.769	0.518	0.472	0.538	0.613	0.658	0.741	0.714	0.725	0.763	0.862	0.909	0.980
3	0.990	1.010	0.962	0.781	0.685	0.658	0.565	0.559	0.535	0.521	0.505	0.532	0.578
4	0.794	0.641	0.452	0.498	0.556	0.552	0.508	0.441	0.474	0.441	0.426	0.353	0.383
5	1.000	1.020	0.980	0.943	0.917	0.885	0.909	0.909	0.901	0.885	0.862	0.813	0.800
6	0.943	0.962	1.000	1.042	1.010	1.020	1.031	1.042	1.053	1.053	1.031	1.010	1.000
7	0.962	1.020	0.971	0.962	0.926	0.893	0.901	0.840	0.787	0.730	0.680	0.568	0.578
8	1.020	0.980	0.990	0.980	1.000	0.971	0.990	1.010	0.962	0.935	0.855	0.806	0.758
9	0.990	1.000	1.087	0.990	0.885	0.885	0.820	0.820	0.769	0.763	0.746	0.645	0.633
10	0.847	0.602	0.498	0.633	0.694	0.730	0.794	0.794	0.820	0.862	0.877	0.877	0.877
11	1.010	1.020	1.010	1.031	0.962	0.935	0.952	0.917	0.935	0.862	0.813	0.725	0.746
12	0.952	0.926	0.962	0.971	0.971	1.010	0.971	0.917	0.971	0.885	0.909	0.806	0.741
13	0.971	0.962	0.962	0.935	0.926	0.926	0.926	0.909	0.943	0.926	0.917	0.769	0.840
14	1.053	1.064	1.053	1.031	1.042	1.042	1.042	1.042	1.010	1.000	1.010	0.943	0.971
15	1.000	0.990	1.020	0.980	0.990	1.020	0.990	0.962	0.935	0.980	0.952	0.885	0.885
16	0.971	0.980	0.971	0.952	0.943	0.962	0.943	0.926	0.943	0.862	0.833	0.585	0.549
17	1.010	0.971	1.010	0.971	0.943	0.971	0.943	0.909	0.870	0.877	0.833	0.775	0.787
18	1.020	1.031	1.000	0.935	0.935	0.926	0.909	0.877	0.885	0.885	0.877	0.775	0.746
19	0.971	1.010	1.031	0.962	0.885	0.840	0.667	0.658	0.585	0.552	0.575	0.568	0.602
20	1.010	1.136	1.250	1.087	1.000	0.952	0.901	0.877	0.813	0.794	0.787	0.746	0.752
21	0.840	0.658	0.621	0.649	0.690	0.730	0.769	0.794	0.800	0.833	0.877	0.877	0.855
22	1.042	1.190	1.235	1.099	0.990	0.980	0.943	0.901	0.909	0.862	0.885	0.855	0.800
23	0.980	1.010	1.000	0.971	0.952	0.926	0.935	0.909	0.909	0.885	0.885	0.885	0.847
24	1.031	1.031	0.971	1.010	1.000	1.020	0.990	0.962	0.926	0.917	0.885	0.813	0.769
25	0.980	0.980	1.000	1.010	0.980	0.971	0.935	0.971	0.917	0.909	0.909	0.833	0.787
26	1.053	1.042	1.010	0.980	0.980	1.000	0.980	0.980	0.952	0.962	0.943	0.926	0.901

TABLE 5 (CONT.)

LINE INDEX DATA

LINE	EARLY M V	MID M V	LATE M V	EARLY F IV	LATE F IV	EARLY G IV	LATE G IV	EARLY K IV	EARLY K IV SMR	EARLY F III	LATE F III	EARLY G III	LATE G III
1	0.820	0.885	1.053	0.463	0.529	0.617	0.813	0.877	0.599	0.450	0.463	0.526	0.794
2	1.010	0.990	1.075	0.585	0.676	0.714	0.826	0.787	0.885	0.585	0.625	0.685	0.758
3	0.714	0.741	0.870	0.654	0.581	0.518	0.474	0.529	0.556	0.735	0.581	0.588	0.488
4	0.521	0.556	0.730	0.526	0.518	0.441	0.400	0.405	0.461	0.524	0.488	0.444	0.391
5	0.893	0.909	0.909	0.935	0.917	0.885	0.847	0.870	0.855	0.935	0.917	0.917	0.901
6	1.000	0.952	0.962	1.000	1.031	1.010	1.010	0.980	0.990	1.031	1.000	1.031	1.020
7	0.680	0.794	0.862	0.893	0.885	0.847	0.735	0.662	0.725	0.926	0.909	0.840	0.719
8	0.833	0.909	0.917	1.000	0.990	0.971	0.962	0.917	0.926	1.010	1.020	0.926	0.935
9	0.741	0.787	0.962	0.862	0.806	0.806	0.685	0.637	0.763	0.901	0.840	0.806	0.641
10	0.909	0.917	0.943	0.645	0.758	0.813	0.909	0.926	0.917	0.649	0.741	0.787	0.917
11	0.840	0.901	0.990	1.020	0.980	0.962	0.833	0.781	0.885	1.010	0.971	0.917	0.813
12	0.769	0.840	0.917	1.000	0.962	0.943	0.877	0.855	0.962	0.962	0.971	0.935	0.909
13	0.855	0.901	0.971	0.943	0.926	0.926	0.893	0.847	0.877	0.943	0.926	0.901	0.885
14	0.935	0.980	1.000	1.031	1.042	0.990	0.990	0.885	1.020	1.020	1.020	0.980	0.952
15	0.855	0.847	0.893	0.952	0.990	0.952	0.885	0.833	0.855	0.952	0.990	0.943	0.901
16	0.417	0.413	0.602	0.917	0.952	0.935	0.885	0.685	0.714	0.935	0.935	0.909	0.862
17	0.787	0.806	0.840	0.962	0.943	0.952	0.870	0.820	0.806	0.990	0.980	0.926	0.877
18	0.730	0.813	0.826	0.917	0.909	0.909	0.862	0.833	0.847	0.926	0.909	0.885	0.909
19	0.769	0.885	0.909	0.893	0.709	0.637	0.493	0.513	0.524	0.943	0.813	0.649	0.503
20	0.820	0.885	0.926	1.010	0.926	0.885	0.794	0.758	0.746	1.053	0.952	0.885	0.752
21	0.917	0.990	1.031	0.680	0.775	0.800	0.870	0.847	0.877	0.690	0.741	0.826	0.862
22	0.840	0.840	0.787	1.020	0.935	0.909	0.833	0.826	0.787	1.042	0.926	0.893	0.862
23	0.917	0.971	1.000	0.952	0.952	0.901	0.870	0.855	0.909	0.962	0.943	0.926	0.855
24	0.855	0.917	0.943	1.010	0.990	0.990	0.935	0.943	0.901	0.990	1.020	0.971	0.943
25	0.901	0.980	1.000	0.962	0.962	0.962	0.917	0.840	0.877	0.962	0.980	0.909	0.885
26	0.935	0.990	1.000	1.031	0.962	0.990	0.990	0.971	0.990	1.042	1.010	1.010	0.980

TABLE 5 (CONT.)

LINE INDEX DATA

LINE	LATE G III SMR	EARLY K III	EARLY K III SMR	LATE K III	LATE K III SMR	EARLY M III	MID M III	LATE M III	HOR. BR.	GLOB. CL. I	GLOB. CL. II	GLOB. CL. VI	POP. II
1	0.901	0.800	0.833	0.763	0.719	0.847	0.769	0.952	0.389	0.680	0.704	0.980	0.800
2	0.741	0.862	0.847	0.820	0.926	0.833	0.840	0.862	0.490	0.709	0.781	0.877	0.885
3	0.529	0.463	0.467	0.513	0.571	0.529	0.524	0.455	1.000	0.833	0.752	0.847	0.662
4	0.455	0.340	0.356	0.361	0.408	0.365	0.389	0.302	0.529	0.680	0.610	0.719	0.568
5	0.909	0.847	0.870	0.826	0.855	0.870	0.926	1.000	1.020	0.990	0.943	0.990	0.980
6	1.053	1.010	0.943	0.962	0.935	0.952	0.909	0.952	1.000	1.000	1.020	0.990	1.010
7	0.806	0.645	0.676	0.606	0.621	0.641	0.690	0.763	0.962	0.943	0.943	1.000	0.917
8	0.971	0.909	0.870	0.893	0.901	0.885	0.926	0.962	1.000	0.990	0.971	1.020	0.971
9	0.752	0.641	0.625	0.621	0.595	0.585	0.578	0.699	1.099	0.971	0.917	0.935	0.885
10	0.943	0.926	1.053	0.980	0.980	0.962	0.962	0.980	0.552	0.820	0.826	0.909	0.893
11	0.855	0.752	0.794	0.719	0.787	0.775	0.800	0.833	1.000	1.000	0.971	0.935	0.980
12	0.990	0.800	1.000	0.833	0.826	0.800	0.813	0.855	0.935	0.943	0.917	0.980	0.943
13	0.917	0.826	0.847	0.806	0.787	0.787	0.800	0.885	0.980	0.971	0.952	0.990	0.909
14	0.926	0.885	0.962	0.877	0.893	0.855	0.893	0.952	1.020	1.053	1.031	0.990	1.053
15	0.885	0.870	0.885	0.862	0.840	0.813	0.763	0.719	1.010	1.010	0.952	0.971	0.990
16	0.952	0.709	0.667	0.549	0.571	0.529	0.444	0.389	0.962	0.952	0.952	0.935	0.943
17	0.917	0.826	0.781	0.813	0.746	0.840	0.833	0.901	0.990	0.990	0.952	0.952	0.952
18	0.862	0.794	0.806	0.758	0.725	0.758	0.676	0.813	1.000	0.990	0.952	0.901	0.917
19	0.508	0.508	0.465	0.529	0.515	0.621	0.709	0.935	0.990	0.917	0.794	0.719	0.741
20	0.813	0.787	0.714	0.752	0.709	0.662	0.787	0.833	1.220	0.990	0.971	0.901	0.909
21	0.833	0.870	0.855	0.855	0.800	0.870	0.862	0.926	0.641	0.847	0.840	0.862	0.885
22	0.833	0.833	0.794	0.820	0.806	0.943	0.833	0.862	1.235	1.000	0.990	0.926	0.952
23	0.855	0.840	0.826	0.826	0.833	0.877	0.909	0.971	1.053	0.971	0.971	0.943	0.943
24	0.952	0.952	0.909	0.893	0.826	0.917	0.935	1.010	1.020	1.010	0.980	1.031	1.000
25	0.901	0.855	0.847	0.840	0.741	0.962	0.862	0.909	1.031	0.971	0.943	0.980	0.980
26	0.952	0.935	0.935	0.962	0.901	1.031	1.020	1.149	0.971	1.010	0.952	0.926	1.010

TABLE 5 (CONT.)

LINE INDEX DATA

LINE	NGC 3031 (M81)	NGC 3115	NGC 3379	NGC 4473	NGC 4594 (M104)	NGC 5194 (M51)	NGC 221 (M32)	NGC 224 (M31)	NGC 584	NGC 1052
1	0.862	0.877	0.806	0.877	0.862	0.800	0.775	0.893	0.926	0.901
2	0.935	0.893	0.909	0.917	0.952	0.862	0.787	0.870	0.943	1.042
3	0.667	0.690	0.680	0.690	0.714	0.775	0.637	0.649	0.855	0.885
4	0.568	0.595	0.562	0.592	0.617	0.658	0.565	0.565	0.763	0.769
5	0.962	0.952	0.909	0.943	0.917	0.885	0.935	0.926	0.943	0.980
6	0.980	0.935	0.990	0.926	0.990	0.990	1.031	1.020	1.031	0.990
7	0.877	0.952	0.952	0.909	0.952	0.962	0.855	0.901	0.885	0.962
8	0.980	0.980	0.980	0.952	1.031	0.971	0.980	0.962	0.962	1.042
9	0.862	0.862	0.862	0.877	0.826	0.926	0.781	0.813	0.901	0.901
10	0.909	0.885	0.943	0.893	0.962	0.840	0.862	0.935	0.926	0.990
11	0.943	1.010	0.952	0.952	0.971	1.020	0.952	0.952	1.042	0.962
12	1.020	0.943	1.031	0.980	1.064	0.909	0.980	1.031	0.962	1.020
13	0.917	0.909	0.885	0.990	0.901	0.893	0.962	0.943	0.952	0.909
14	1.042	1.010	1.031	1.020	1.020	1.031	1.042	1.031	0.990	0.980
15	0.980	1.010	0.980	0.971	1.087	0.980	0.962	1.000	1.010	1.010
16	0.833	0.855	0.855	0.870	0.820	0.909	0.909	0.885	0.926	0.870
17	0.885	0.952	0.935	0.909	0.952	0.935	0.909	0.926	0.962	0.952
18	0.917	0.935	0.909	0.926	0.935	0.926	0.893	0.909	0.980	0.962
19	0.667	0.719	0.649	0.714	0.725	0.758	0.676	0.709	0.735	0.746
20	0.847	0.917	0.847	0.935	0.909	0.909	0.870	0.840	0.0	0.893
21	0.926	0.0	0.0	0.862	0.0	0.893	0.855	0.893	0.0	0.0
22	0.962	0.0	0.917	0.935	0.0	0.0	0.909	0.952	1.031	0.943
23	0.926	0.926	0.926	0.935	0.943	0.952	0.893	0.893	0.901	0.935
24	0.952	0.943	0.943	0.962	0.935	0.962	0.971	0.935	0.990	0.943
25	0.909	0.943	0.952	0.971	0.943	0.943	0.935	0.917	0.943	0.962
26	0.971	1.031	0.990	1.000	1.020	1.031	1.000	1.000	1.000	1.020

TABLE 5 (CONT.)

LINE INDEX DATA

LINE	OB V	LATE B V	EARLY A V	LATE A V	EARLY F V	MID F V	LATE F V	EARLY G V	MID G V	LATE G V	EARLY K V	MID K V	LATE K V
27	0.990	0.980	0.990	1.000	0.926	0.935	0.952	0.935	0.935	0.943	0.917	0.917	0.813
28	0.877	0.943	0.943	1.000	1.000	0.980	1.042	0.990	1.020	1.075	1.075	1.111	1.087
29	1.020	1.087	1.064	1.053	1.010	1.064	1.064	1.064	1.042	1.053	1.010	1.031	1.053
30	1.053	1.064	1.020	0.980	0.962	0.962	0.971	0.943	0.935	0.885	0.840	0.826	0.847
31	1.000	1.075	1.031	0.990	0.990	0.962	0.952	0.926	0.909	0.885	0.877	0.820	0.833
32	0.980	0.980	0.980	0.990	0.943	0.962	0.980	0.971	0.935	0.935	0.935	0.909	0.901
33	0.962	0.971	0.990	0.980	0.962	0.980	0.943	0.952	0.917	0.962	0.917	0.847	0.926
34	0.962	1.000	0.980	0.980	0.962	0.980	0.980	0.990	0.952	0.980	0.990	0.952	0.943
35	0.990	1.010	0.990	1.010	1.000	0.962	0.990	0.971	0.962	1.010	0.962	0.926	0.980
36	0.820	0.694	0.595	0.671	0.709	0.730	0.800	0.794	0.847	0.885	0.901	0.893	0.935
37	0.980	1.010	1.031	1.000	0.971	0.962	0.990	1.010	0.980	0.990	0.962	0.901	0.909
38	0.980	0.885	1.000	0.980	0.962	0.962	0.971	0.952	0.926	0.909	0.926	0.870	0.877
39	1.010	0.980	0.990	0.962	0.980	0.990	1.000	0.980	1.010	0.943	0.952	0.926	0.943
40	0.943	0.971	0.980	0.990	1.000	0.917	0.990	0.962	0.980	0.980	0.962	0.962	0.971
41	1.010	0.990	0.935	0.952	0.990	0.962	1.000	0.962	0.926	0.943	0.962	0.935	0.901
42	1.010	1.000	1.020	0.990	0.893	0.943	1.000	0.952	0.926	0.990	0.962	0.917	0.943
43	0.980	1.010	0.952	0.962	0.971	0.971	0.885	0.952	0.909	0.870	0.877	0.917	0.952
44	0.990	1.010	0.952	0.971	0.909	0.909	0.935	0.909	0.877	0.877	0.855	0.741	0.752
45	1.000	0.909	0.980	1.031	1.031	1.020	1.000	0.990	0.962	0.917	0.855	0.714	0.794
46	1.010	0.980	1.031	0.971	0.971	0.990	0.980	0.980	0.990	0.917	0.855	0.694	0.730
47	0.971	1.010	1.020	1.010	1.000	0.971	0.980	0.962	0.990	0.971	0.909	0.935	0.833
48	1.010	0.990	0.990	0.943	0.917	0.926	0.909	0.917	0.893	0.862	0.820	0.794	0.855
49	1.031	1.010	1.020	1.010	1.053	1.020	1.000	0.971	0.952	0.926	0.962	0.870	0.893
50	0.980	1.031	0.980	0.971	0.943	0.935	0.893	0.935	0.901	0.855	0.855	0.787	0.862
51	1.075	1.042	1.010	1.031	1.031	1.020	0.971	1.020	0.971	0.980	0.952	0.926	0.943
52	1.031	1.064	1.031	1.042	0.971	1.031	1.000	0.962	0.917	0.943	0.926	0.877	0.943

TABLE 5 (CONT.)

LINE INDEX DATA

LINE	EARLY M V	MID M V	LATE M V	EARLY F IV	LATE F IV	EARLY G IV	LATE G IV	EARLY K IV	EARLY K IV SMR	EARLY F III	LATE F III	EARLY G III	LATE G III
27	0.870	0.885	0.909	0.990	0.962	0.926	0.962	0.917	0.885	0.980	0.962	0.935	0.935
28	1.176	1.075	1.111	0.971	0.990	1.020	1.064	1.111	1.087	0.990	0.980	0.971	1.087
29	1.010	1.010	0.980	1.163	1.124	1.020	1.031	1.053	1.064	1.205	1.064	1.075	1.053
30	0.833	0.877	0.926	0.980	0.962	0.917	0.917	0.840	0.840	0.962	0.943	0.943	0.893
31	0.855	0.980	0.990	0.962	0.943	0.901	0.901	0.820	0.833	0.980	0.952	0.917	0.893
32	0.926	1.042	1.087	0.990	0.962	0.926	0.901	0.855	0.893	0.952	0.943	0.943	0.901
33	0.935	1.000	1.064	1.000	1.000	0.926	0.917	0.862	0.855	1.000	0.962	0.952	0.926
34	0.971	0.990	0.990	0.990	1.000	0.962	0.935	0.952	0.935	0.980	0.962	0.962	0.971
35	0.901	0.909	0.909	1.000	1.000	0.980	0.971	0.980	0.962	1.031	0.990	0.990	0.980
36	1.010	1.000	0.980	0.758	0.787	0.813	0.901	0.909	0.870	0.676	0.781	0.877	0.935
37	0.943	0.990	0.962	0.980	1.000	0.952	0.962	1.042	1.000	1.031	0.990	1.020	0.990
38	0.741	0.637	0.571	0.971	0.943	0.962	0.943	0.877	0.917	0.962	0.962	0.962	0.926
39	1.031	0.952	0.862	0.971	0.952	0.962	0.962	0.962	1.000	0.971	0.990	0.962	0.962
40	0.901	0.917	0.901	1.000	0.962	0.971	0.926	0.935	0.971	0.990	0.952	0.971	0.971
41	0.901	0.901	0.952	0.971	0.943	0.943	0.943	0.962	0.909	0.990	0.971	0.926	0.935
42	0.962	0.980	0.980	0.971	0.943	0.943	0.943	0.943	0.971	0.943	0.971	0.952	0.935
43	0.893	0.909	0.862	0.980	0.917	0.926	0.943	0.840	0.840	0.990	0.943	0.877	0.885
44	0.935	0.990	0.990	0.962	0.962	0.893	0.862	0.877	0.877	0.943	0.943	0.943	0.901
45	0.709	0.685	0.641	1.042	0.990	1.000	0.901	0.877	0.870	1.031	1.010	1.010	0.952
46	0.585	0.658	0.602	0.971	1.000	1.000	0.943	0.820	0.909	0.980	0.980	0.935	0.935
47	0.885	0.952	0.926	0.980	0.980	0.943	0.943	0.826	0.893	1.000	0.980	0.926	0.893
48	0.806	0.833	0.800	0.980	0.952	0.893	0.855	0.820	0.847	0.971	0.926	0.870	0.820
49	0.917	0.971	0.943	0.980	1.010	0.943	0.943	0.917	0.909	1.010	1.020	0.952	0.926
50	0.862	0.943	0.935	0.943	0.917	0.909	0.885	0.855	0.847	0.909	0.943	0.901	0.885
51	0.926	0.926	0.909	0.990	1.010	1.020	1.000	0.952	0.943	1.000	1.020	1.000	1.000
52	0.893	0.943	0.943	1.020	1.010	0.971	0.952	0.870	0.870	1.020	0.990	0.971	0.926

TABLE 5 (CONT.)

LINE INDEX DATA

LINE	LATE G III SMR	EARLY K III	EARLY K III SMR	LATE K III	LATE K III SMR	EARLY M III	MID M III	LATE M III	HOR. BR.	GLOB. CL. I	GLOB. CL. II	GLOB. CL. VI	POP. II
27	0.901	0.901	0.926	0.901	0.775	1.075	0.893	1.042	1.020	0.980	0.952	0.980	1.000
28	1.064	1.087	1.136	1.099	0.990	1.149	0.971	0.980	0.952	0.990	0.971	1.064	0.990
29	0.870	0.971	1.031	1.075	1.020	1.042	1.010	0.962	0.962	1.042	1.031	1.053	1.099
30	0.833	0.909	0.820	0.800	0.847	0.806	0.794	0.758	1.075	1.000	0.971	0.893	0.990
31	0.855	0.893	0.794	0.769	0.794	0.781	0.917	0.990	0.971	1.020	0.935	0.952	0.971
32	0.909	0.870	0.862	0.870	0.885	0.926	1.429	2.174	1.000	1.000	0.980	0.935	0.980
33	0.901	0.952	0.813	0.870	0.820	0.877	0.990	1.176	1.075	1.010	1.042	1.010	1.020
34	0.935	0.909	0.862	0.926	0.877	0.917	0.943	0.971	1.031	1.010	1.000	1.010	0.962
35	0.926	0.971	0.917	0.943	0.962	0.952	0.862	0.787	0.990	1.020	1.000	0.926	0.980
36	0.840	0.917	0.926	0.971	0.962	0.917	0.826	0.855	0.671	0.862	0.847	0.847	0.909
37	1.042	1.020	1.064	0.962	1.010	0.990	1.042	1.075	0.980	1.000	1.000	1.099	1.000
38	1.000	0.935	0.909	0.877	0.870	0.763	0.455	0.295	0.990	0.980	0.952	0.926	0.962
39	0.952	0.962	0.926	0.962	0.962	0.943	0.820	0.741	1.020	0.980	0.971	0.943	1.010
40	0.990	0.952	0.990	0.926	0.980	0.917	0.893	0.758	1.042	0.990	0.971	0.990	0.980
41	1.020	0.943	0.952	0.917	0.885	0.885	0.794	0.794	1.053	0.990	0.962	0.962	0.990
42	0.980	0.971	0.917	0.909	0.885	0.962	0.935	0.893	1.087	1.000	1.000	1.053	1.000
43	0.909	0.926	0.862	0.926	0.862	0.877	0.800	0.735	1.042	0.909	0.990	0.909	0.935
44	0.893	0.820	0.806	0.820	0.893	0.775	0.775	0.775	0.962	1.031	0.962	0.877	0.962
45	1.020	0.877	0.893	0.833	0.826	0.763	0.758	0.599	0.990	1.020	1.010	0.980	1.053
46	0.971	0.893	0.847	0.694	0.758	0.704	0.714	0.694	0.990	0.877	0.990	0.926	0.935
47	0.917	0.877	0.855	0.855	0.870	0.826	0.763	0.752	0.990	1.000	0.962	0.962	0.971
48	0.840	0.847	0.725	0.787	0.741	0.800	0.769	0.758	1.000	0.990	0.943	0.826	0.917
49	1.042	0.909	0.806	0.885	0.806	0.917	0.990	0.980	1.010	1.020	0.980	0.877	0.980
50	0.855	0.862	0.820	0.862	0.840	0.901	0.980	1.000	1.031	0.980	0.952	0.952	0.962
51	0.962	0.990	0.971	0.943	0.952	0.952	0.917	0.885	0.990	1.031	1.020	1.000	1.010
52	0.926	0.909	0.840	0.855	0.787	0.885	0.935	1.010	0.990	1.042	1.000	0.935	1.000

TABLE 5 (CONT.)

LINE INDEX DATA

LINE	NGC 3031 (M81)	NGC 3115	NGC 3379	NGC 4473	NGC 4594 (M104)	NGC 5194 (M51)	NGC 221 (M32)	NGC 224 (M31)	NGC 584	NGC 1052
27	0.917	0.909	0.885	0.926	0.909	0.917	0.901	0.877	0.952	0.909
28	1.053	1.064	1.010	1.020	1.042	1.000	1.053	1.010	1.031	1.064
29	1.064	1.075	1.075	1.042	1.075	1.064	1.075	1.064	1.000	1.010
30	0.935	0.926	0.917	0.935	0.926	0.917	0.893	0.885	0.917	0.926
31	0.917	0.952	0.962	0.901	0.952	0.943	0.901	0.877	0.926	0.885
32	0.971	0.980	1.020	0.990	1.010	0.935	0.926	0.943	0.952	1.010
33	0.935	0.990	1.020	0.943	0.962	0.917	0.885	0.917	0.971	0.980
34	0.971	0.971	1.031	0.971	0.952	0.962	0.990	0.971	0.971	0.980
35	0.971	0.943	0.926	0.980	0.980	0.917	0.962	0.971	0.980	0.952
36	0.962	0.917	0.952	0.935	0.943	0.926	0.943	0.962	0.909	0.0
37	0.971	0.971	0.943	0.971	0.935	1.000	1.010	0.962	0.926	0.926
38	0.990	0.926	0.952	0.952	0.980	0.990	0.893	0.917	0.943	0.0
39	1.010	0.943	1.020	1.053	0.990	0.0	0.980	0.962	0.990	0.0
40	0.0	1.020	1.010	0.990	1.000	0.0	1.000	0.971	0.962	0.0
41	1.000	0.962	1.010	0.971	1.000	0.971	1.000	0.962	0.935	0.971
42	0.962	1.087	1.111	1.075	0.926	0.980	0.943	0.962	0.962	0.901
43	0.935	0.990	0.980	0.952	0.980	0.962	0.862	0.901	0.952	0.909
44	0.962	0.877	0.909	0.943	0.877	0.877	0.885	0.826	0.840	0.794
45	0.847	0.847	0.877	0.870	0.813	0.0	0.952	0.833	0.870	0.800
46	0.935	0.926	0.962	0.926	0.926	0.0	0.862	0.893	0.893	0.971
47	1.010	0.952	1.000	1.010	0.952	0.990	0.901	0.943	0.962	0.952
48	0.909	0.885	0.893	0.943	0.833	0.901	0.813	0.820	0.877	0.862
49	1.010	0.990	1.042	0.990	0.952	1.010	0.962	0.935	0.935	0.943
50	0.909	0.917	0.943	0.935	0.909	0.935	0.893	0.885	0.917	0.909
51	1.042	1.000	0.0	1.010	0.971	0.980	0.980	0.971	1.010	1.010
52	0.980	0.943	0.971	0.909	0.980	0.952	0.962	0.943	0.962	0.952

TABLE 5 (CONT.)

LINE INDEX DATA

LINE	OB V	LATE B V	EARLY A V	LATE A V	EARLY F V	MID F V	LATE F V	EARLY G V	MID G V	LATE G V	EARLY K V	MID K V	LATE K V
53	0.893	0.952	0.926	0.935	0.943	0.943	0.943	0.952	0.962	0.971	0.980	0.962	0.962
54	1.000	1.020	1.020	0.952	0.952	0.952	0.943	0.952	0.935	0.909	0.885	0.877	0.877
55	1.010	1.031	1.042	1.053	1.042	1.042	1.053	1.020	1.000	0.980	1.000	0.990	1.075
56	0.935	1.010	0.971	1.000	0.990	0.990	0.971	0.980	0.962	1.000	0.943	0.885	0.971
57	1.010	1.000	1.010	1.020	0.990	1.000	1.000	1.020	0.980	1.010	1.053	1.010	0.990
58	1.010	1.010	1.000	1.000	0.980	0.980	0.971	0.971	0.962	0.980	0.980	0.943	1.010
59	0.952	1.010	0.962	0.935	0.917	0.943	0.926	0.909	0.885	0.855	0.775	0.610	0.602
60	0.962	0.971	1.010	1.010	1.000	1.010	0.990	1.000	1.000	0.980	1.031	0.943	1.020
61	1.042	1.042	1.031	1.010	0.990	1.075	1.020	1.020	1.064	1.010	1.053	1.053	1.087
62	0.971	1.010	0.980	0.990	1.031	1.010	1.000	0.980	0.962	1.087	0.990	1.075	1.111
63	1.000	1.031	0.980	1.010	1.020	1.020	0.971	1.000	0.980	0.962	0.980	0.971	0.935
64	1.020	0.990	0.990	0.962	0.952	0.962	0.952	0.962	0.952	0.926	0.909	0.806	0.781
65	0.962	1.031	1.000	1.042	0.962	1.020	1.020	1.020	1.042	1.042	1.020	1.031	1.064
66	1.020	1.010	0.990	1.000	1.031	1.031	0.990	1.031	1.031	1.010	1.010	1.020	1.020
67	1.010	0.980	1.042	1.000	0.962	1.000	0.980	1.010	0.980	1.020	1.000	0.971	1.010
68	1.000	1.000	1.020	1.010	1.020	1.010	1.031	1.031	1.042	1.010	1.020	0.935	1.020
69	1.010	1.000	1.010	0.980	0.962	0.980	0.935	0.935	0.943	0.909	0.943	0.935	0.893
70	0.971	0.952	0.870	0.917	0.980	0.952	0.962	0.943	0.990	0.917	1.000	0.980	0.962
71	0.971	0.962	0.926	1.020	1.010	0.962	0.962	0.952	0.917	0.971	0.971	0.990	0.926
72	1.000	1.053	1.053	1.000	0.980	1.010	1.064	1.020	1.064	0.980	0.990	1.000	1.031
73	1.031	1.075	1.000	1.010	1.042	1.064	1.075	1.075	1.099	1.020	1.000	1.075	1.053
74	1.010	0.943	0.943	0.971	1.000	0.971	1.020	1.053	0.943	0.990	1.000	0.952	0.990

TABLE 5 (CONT.)

LINE INDEX DATA

LINE	EARLY M V	MID M V	LATE M V	EARLY F IV	LATE F IV	EARLY G IV	LATE G IV	EARLY K IV	EARLY K IV SMR	EARLY F III	LATE F III	EARLY G III	LATE G III
53	0.840	0.699	0.694	0.990	0.971	0.971	0.990	0.980	1.000	0.962	0.943	1.000	0.980
54	0.980	0.990	1.064	0.962	0.971	0.909	0.909	0.893	0.862	0.962	0.935	0.893	0.840
55	0.980	0.862	0.870	1.010	1.064	1.020	1.020	1.020	1.042	1.020	1.042	1.010	1.000
56	0.943	0.952	0.926	1.000	0.943	0.962	0.943	0.952	0.909	1.000	0.952	0.952	0.926
57	0.935	0.833	0.847	1.064	1.064	1.031	1.075	1.064	1.020	1.042	1.010	1.064	1.031
58	0.926	0.885	0.862	1.020	0.990	0.971	0.980	0.980	0.990	0.990	0.971	1.020	0.962
59	0.568	0.578	0.654	0.935	0.935	0.901	0.870	0.735	0.746	0.909	0.901	0.870	0.833
60	0.935	0.971	0.952	0.962	1.000	0.990	0.980	0.980	0.990	0.962	0.952	0.980	0.980
61	1.010	0.971	0.952	1.000	1.010	1.020	1.053	0.990	1.042	1.010	1.031	1.010	1.042
62	1.111	1.042	1.064	0.943	1.031	0.990	1.010	1.000	1.020	0.971	0.962	1.031	1.031
63	0.943	0.885	0.855	0.962	0.990	0.962	1.010	0.971	0.952	0.962	1.020	0.980	0.971
64	0.806	0.935	0.962	1.020	1.000	0.971	0.952	0.877	0.901	0.971	0.962	0.962	0.952
65	1.000	1.000	1.020	1.031	1.042	1.020	1.000	1.053	1.087	1.031	1.000	1.020	1.020
66	0.990	1.000	0.952	0.962	0.980	1.020	1.020	1.010	1.000	1.010	1.031	1.042	1.042
67	1.020	1.000	0.971	1.031	1.075	1.000	1.010	1.020	0.980	1.031	1.031	1.010	0.943
68	1.010	0.962	0.952	1.010	0.990	1.031	0.990	1.000	0.990	1.020	1.031	0.980	1.000
69	0.901	0.870	0.885	1.010	0.990	0.971	0.901	0.917	0.909	0.980	0.943	0.962	0.901
70	0.980	0.901	0.917	0.980	1.000	0.962	0.980	0.926	0.952	0.952	0.962	0.980	1.000
71	1.010	1.042	1.099	0.990	0.962	0.952	0.926	0.962	0.926	1.000	1.000	0.962	0.962
72	0.990	0.917	0.885	1.149	0.962	1.042	1.020	1.031	1.000	1.075	1.075	1.031	1.075
73	1.124	1.099	1.124	1.064	1.064	1.031	1.042	1.136	1.053	1.087	1.064	1.042	1.053
74	0.909	0.917	0.917	1.010	0.952	1.000	0.962	0.971	0.952	0.971	0.926	0.952	0.990

TABLE 5 (CONT.)

LINE INDEX DATA

LINE	LATE G III SMR	EARLY K III	EARLY K III SMR	LATE K III	LATE K III SMR	EARLY M III	MID M III	LATE M III	HOR. BR.	GLOB. CL. I	GLOB. CL. II	GLOB. CL. VI	POP. II
53	1.031	0.980	1.010	0.943	1.010	0.840	0.694	0.592	1.000	0.990	0.980	1.010	0.952
54	0.758	0.840	0.847	0.877	0.847	0.885	1.020	1.053	1.020	0.990	0.901	0.962	1.020
55	0.971	1.064	1.042	1.031	1.053	0.971	0.862	0.877	1.031	1.000	1.053	1.020	1.020
56	0.943	0.901	0.820	0.885	0.877	0.870	0.935	0.909	0.962	0.980	0.962	0.862	1.020
57	1.111	1.053	1.010	1.010	1.031	0.952	0.775	0.826	1.031	1.000	1.000	1.099	1.053
58	0.980	0.990	0.980	0.943	0.917	0.909	0.746	0.709	1.010	1.010	1.020	0.917	1.010
59	0.870	0.813	0.719	0.758	0.676	0.806	0.935	0.952	0.980	0.917	0.943	0.840	0.952
60	0.952	1.010	0.980	0.935	0.971	0.980	0.917	0.990	1.020	0.971	1.010	1.064	1.000
61	1.124	1.010	1.000	1.053	1.099	1.031	1.000	0.926	1.020	0.962	1.010	0.926	1.000
62	0.990	0.980	1.031	1.020	0.980	1.000	1.010	1.000	1.010	1.042	1.010	0.980	1.010
63	1.031	1.020	1.020	0.943	0.980	0.885	0.769	0.758	0.990	1.000	1.020	0.962	0.990
64	0.971	0.901	0.877	0.909	0.926	0.909	0.943	0.990	1.064	0.990	0.935	0.926	0.990
65	1.053	1.020	1.053	1.031	1.010	0.980	1.053	1.000	1.020	0.980	1.064	1.064	1.020
66	1.020	1.010	1.020	0.980	1.042	0.943	0.909	0.893	0.962	0.990	1.042	0.980	0.962
67	0.980	0.952	1.064	0.990	0.901	0.935	0.926	0.901	0.990	0.990	1.042	0.962	1.042
68	0.990	0.990	0.926	1.010	0.962	0.962	0.935	0.917	1.000	1.010	1.010	1.075	1.031
69	0.855	0.901	0.943	0.909	0.909	0.909	0.962	0.877	1.010	0.952	0.909	0.917	0.952
70	0.952	0.980	0.935	0.926	0.990	0.917	0.885	0.870	0.926	0.990	1.010	0.990	1.000
71	0.962	0.971	0.952	0.952	0.935	0.980	1.031	1.111	0.952	0.980	0.980	0.962	0.980
72	0.935	1.010	1.000	1.099	0.971	0.980	0.926	0.943	0.990	0.901	0.980	0.926	0.990
73	1.075	1.064	1.149	1.099	1.042	1.136	1.042	1.042	0.952	1.099	1.031	1.031	1.010
74	0.935	0.990	1.000	0.952	1.031	0.943	0.952	1.020	1.031	0.962	0.980	1.020	1.010

TABLE 5 (CONT.)

LINE INDEX DATA

LINE	NGC 3031 (M81)	NGC 3115	NGC 3379	NGC 4473	NGC 4594 (M104)	NGC 5194 (M51)	NGC 221 (M32)	NGC 224 (M31)	NGC 584	NGC 1052
53	1.000	0.0	0.0	0.0	0.0	1.042	0.980	0.990	0.926	0.893
54	0.909	0.926	0.909	0.943	0.909	0.971	0.909	0.901	0.917	0.870
55	1.010	1.010	1.010	0.971	1.000	1.053	1.000	1.042	1.042	1.010
56	0.926	0.980	0.980	0.952	0.962	0.962	0.935	0.971	0.943	1.031
57	1.000	1.042	1.031	0.990	0.990	1.031	0.990	1.010	1.000	1.000
58	0.962	0.980	0.935	0.893	0.990	0.917	0.962	0.962	0.0	0.943
59	0.775	0.813	0.806	0.833	0.833	0.847	0.833	0.741	0.840	0.735
60	1.010	1.010	1.000	0.943	1.020	0.962	0.971	0.980	0.971	1.010
61	1.042	0.0	1.020	1.031	1.020	1.075	1.099	1.000	1.064	1.042
62	0.980	0.952	0.980	1.031	0.952	0.990	0.990	0.971	0.962	1.075
63	0.990	0.935	0.980	0.952	0.962	1.010	0.962	0.952	1.031	1.020
64	0.952	0.990	0.990	1.000	0.990	1.031	0.943	0.943	0.952	0.962
65	1.053	1.000	0.990	1.042	1.010	0.952	1.064	1.010	1.010	1.087
66	1.020	1.000	0.962	1.000	0.971	0.962	0.990	1.010	1.031	0.990
67	1.010	1.031	0.971	0.990	0.990	0.971	1.010	1.000	0.962	1.087
68	1.020	0.971	0.980	1.053	1.000	0.990	0.990	0.971	0.980	1.010
69	0.962	0.990	0.971	0.935	0.952	0.971	0.917	0.909	1.000	1.020
70	0.0	1.010	0.962	1.000	0.0	0.0	0.962	0.990	1.020	0.0
71	0.0	1.042	1.075	1.031	0.0	0.0	0.990	1.020	1.020	0.0
72	0.0	0.962	0.935	0.952	0.0	0.0	1.064	1.000	1.031	0.0
73	0.0	1.053	1.020	1.020	0.0	0.0	1.031	0.990	1.020	0.0
74	0.990	0.990	1.010	1.010	0.971	1.000	0.952	0.971	1.010	1.020

for all the star groups and galaxies are listed in Table 5. An entry of 0.0 in Table 5 indicates an index contaminated by night sky features, by emission lines in the object, or by film flaws.

V. SYNTHESIS PROCEDURE

Previous analytic methods of galaxy population synthesis have been shown to be highly sensitive to noise in the data (Williams 1976a, hereafter Paper I). In the present work, the number of degrees of freedom available to the models has been drastically restricted to reduce such sensitivity. The stellar populations are described by a series of power laws with eight parameters, as follows:

Main sequence:
$$N(m) = P_3^{P_1}\, m^{-P_1} \qquad m \geq P_3$$
$$= P_3^{P_2}\, m^{-P_2} \qquad m \leq P_3$$

Subgiant branch:
$$N(x) = P_5\, x^{P_4} \qquad x \leq P_3'$$
$$= P_5\, P_3'^{P_4}\, 10^{10(P_3'-x)} \qquad x > P_3'$$

Giant branch:
$$N(x) = P_6\, x^{P_4} \qquad x \leq P_3'$$
$$= P_6\, P_3'^{P_4}\, 10^{10(P_3'-x)} \qquad x > P_3'$$

Normal abundance: $N_{NOR}(x) = (1.0-P_7)\, N(x)$

SMR abundance: $N_{SMR}(x) = P_7\, N(x)$

Others: $N(y) + P_8\, y$

The class "others" refers to the metal poor groups discussed above. The independent variable for the main sequence is stellar mass. For the evolved stars, log x is approximately proportional to the effective temperature. For " others", y is approximately proportional to the number of metal poor stars in our galaxy. The value of the independent variable for each group is listed in Table 2. P_3' is the value of x for evolved stars of the same spectral type as dwarfs with $m = P_3$. The relation between P_3 and P_3' is:

$$P_3' = -0.04387 - \frac{0.2787}{\log P_3 - 0.2631}$$

Thus P_1 is the slope of the upper main sequence, P_2 the slope of the lower main sequence, and P_3 the main sequence turnoff. P_4 is the slope of the evolved branches, P_5 the ratio of subgiants to main sequence, and P_6 the ratio of giants to main sequence. P_7 is the fraction of evolved stars which are "super metal rich", and P_8 is the number of metal poor stars. Typical values of the parameters for the solar neighborhood are listed in Table 6; these values are from Blaauw (1965).

A computer algorithm has been devised which finds that set of values for the eight parameters which minimizes the residual difference between the observed galaxy and the computed model. For a set of initial values of the parameters, the number of stars in each group is calculated. The

composite line indices for this model are then:

$$C_i = \frac{\sum_j S_{ij} F_{ij} N_j}{\sum_j F_{ij} N_j} \quad ,$$

where C_i is the i^{th} composite line index, S_{ij} is the value of the i^{th} line index for the j^{th} star group, F_{ij} is the flux of the j^{th} type of star at the i^{th} wavelength, and N_j is the number of stars of type j in the model. (The fluxes F_{ij} have been compiled from Turnrose (1975), Christensen (1972), and O'Connell (1970).) The residual for this model is then:

$$R = \sqrt{\frac{\sum_i w_i (O_i - C_i)^2}{\sum_i w_i}} \quad ,$$

where R is the residual, w_i is a weighting factor for the i^{th} line, and O_i is the observed galaxy index for the i^{th} line. The derivative $\frac{\partial R}{\partial P_n}$ for the n^{th} parameter is estimated, and that parameter is decreased (increased) by a small amount if the sign of the derivative is positive (negative). This procedure is iterated until none of the parameters can undergo a fractional change of more than 10^{-4} without increasing the total residual. This converged model is termed the optimal parameterized model.

There is a simple geometric interpretation of this synthesis algorithm. The models fall on an eight-dimensional hypersurface in a nine-dimensional space, eight of whose dimensions are the values of the eight parameters, with the ninth dimension chi squared for the fit. The algorithm evaluates the gradient of this surface at the current point and moves the model down the slope of the surface towards the minimum. The algorithm steps its way downhill until it is so close to the minimum that even a very small step causes it to overshoot the minimum.

To explore the sensitivity of this method of population synthesis to noise, an investigation similar to that of paper I has been performed. A distribution of stars (termed a pseudo-galaxy) similar to Faber's (1972) basic model of M31 has been constructed; it is the solid curve in figure 1. The optimal parameterized model for this pseudo-galaxy is the set of open circles in figure 1. The discrepancies between the fit and the pseudo-galaxy are discussed below. The pseudo-galaxy is then perturbed with 5% randomly distributed noise, and again modeled; the solution to these perturbed data is the set of crosses in figure 1. It is clear that the power law parameterization has stabilized the model against the influence of noise.

The discrepancies between the curve and the points in figure 1 result from the form of the parameterization. The

Figure 1

The effects of noise on the optimal parameterized model. The logarithm of the relative number of stars used is shown for each star group. Points at the bottom boundary of the figure represent $N \leq 10^{-10}$. HB refers to horizontal branch stars, GC to globular clusters (metal content increases to right), and PII to Population II giants. The solid curve is the pseudo-galaxy with no noise. The open points are the parameterized fit to it. The crosses are the parameterized fit to the pseudo-galaxy with 5 % noise.

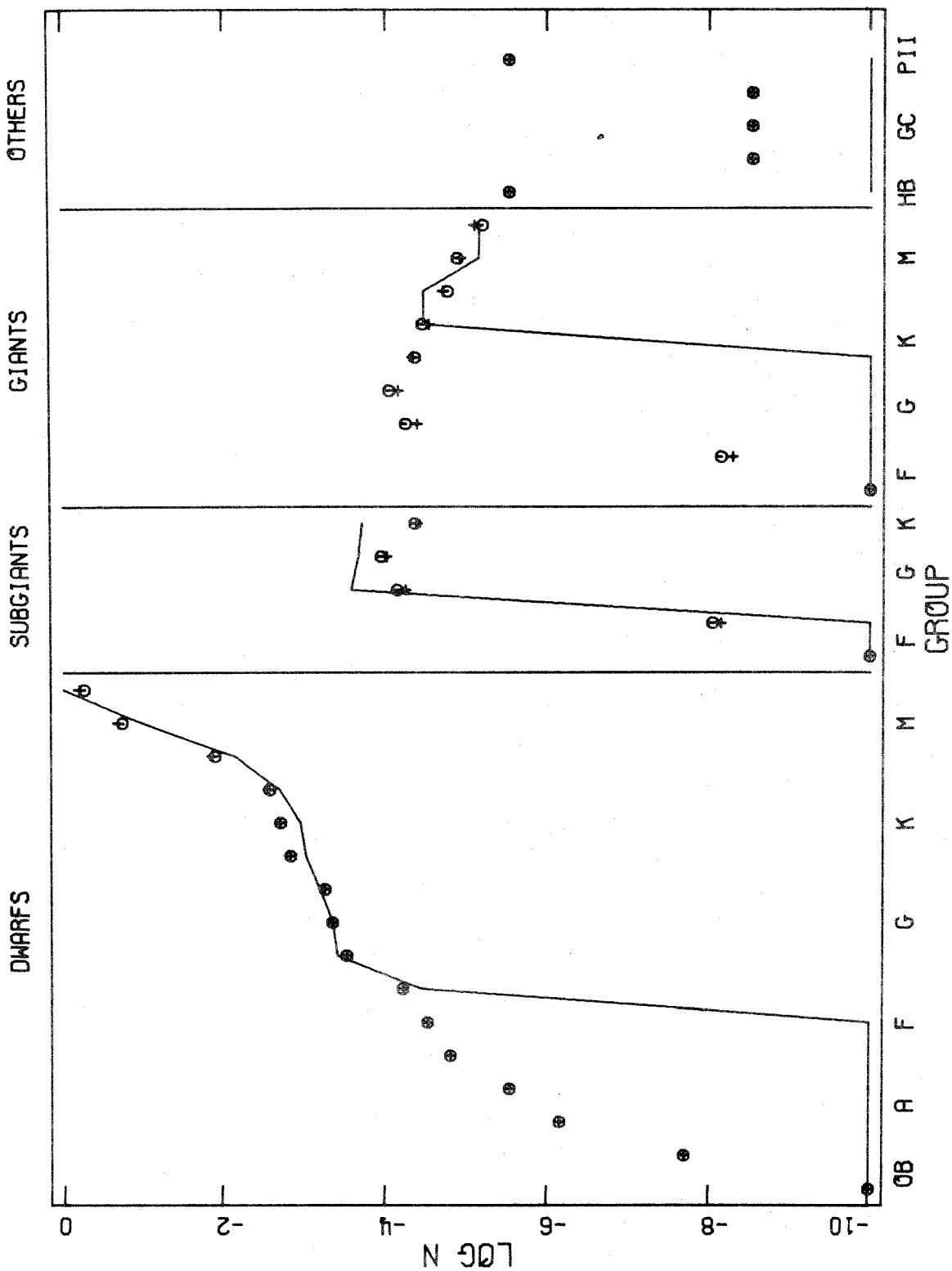
DWARFS
SUBGIANTS
GIANTS
OTHERS
LOG N
0
-2
-4
-6
-8
-10
OB A F G K M F G K M F G K M HB GC PII
GROUP

subgiant and giant branches are required to extend to the main sequence turnoff, thus causing too many G giants to be used; the model compensates for this by reducing the number of subgiants, which are primarily of type G. The slope of the upper main sequence was decreased to fit the number of late F dwarfs; this causes too many early dwarfs to be present. These early dwarfs contribute less than 2 percent of the total light of the model. They are compensated for by the introduction of weak-lined metal poor stars, which contribute 4 percent of the light.

While the above discrepancies are small, it is clear that the details of the optimal parameterized model depend upon the specific form of the parameterization. This dependence is the price that must be paid for eliminating the sensitivity to noise. Of more importance than the optimal model are the limits that can be put upon the stellar distribution. These limits are estimated by varying each parameter from its optimal value until the reduced chi square statistic for the fit reaches a value corresponding to the 70 percent and 95 percent confidence intervals (one and two standard deviations). These limits describe the envelopes of the stellar distributions which are acceptable fits to the data; all distributions within the envelopes are equally acceptable.

The parameterization scheme outlined above is cast in terms of observational quantities - slopes of sequences and

ratios between sequences. Other forms of parameterization could be constructed which are cast in theoretical terms - initial mass functions, stellar birthrate functions, etc. Such alternative parameterizations will not be explored in this paper. As will be seen below, the parameterization used here is adequate to fit the data to within the observational errors.

VI. RESULTS FOR INDIVIDUAL GALAXIES

The optimal parameterized model for each galaxy, along with the one and two standard deviation limits for each parameter is listed in Table 6. The models are plotted in figure 2. Figures comparing the synthesized spectra to the actual galaxy spectra will be presented in a subsequent paper (Williams 1976b). In the sections below, the characteristics of the model for each galaxy are discussed, and the models are compared with results by other authors.

a) M31

The model for M31 is shown in figure 2a. It has a strong contribution from the evolved stars, with giants providing 49 percent of the V band light and subgiants 5 percent. Metal poor stars provide 27 percent of the light. The main sequence, with 18 percent of the light and 99.5 percent of the mass is much steeper than the main sequence in the solar neighborhood. The main-sequence turnoff is at

late G, corresponding to an age of $8 \pm 1 \times 10^9$ years (Rood 1972). The M/L for the model is 46 ±18 in V light. The M/L ratio is strongly dependent upon the number of late M dwarfs, which contribute only 10 percent of the light, and is thus not well determined by population synthesis. The model uses a large fraction of SMR stars, yet is over 10 percent too weak at the Na D and Mg b lines. It thus appears that the stars in the nucleus of M31 have stronger metal lines than any in the solar neighborhood.

This model is similar in several respects to earlier models by Spinrad and Taylor (1971) and by Faber (1972). The distribution of light between the main sequence and evolved branches, the steep slope of the lower main sequence, the mass-to-light ratio, and the high metallicity of the giants, agree well with their models. Spinrad and Taylor found an earlier main sequence turnoff and no contributions by metal poor stars. Thus the population found here appears similar, but older, than previous models. Also the present model includes a sizable fraction of M giant stars, contributing about as much light as M dwarfs, while the previous models allowed no M giants. This M giant contribution appears sufficient to produce the infrared CO band strength observed by Baldwin, et al. (1973).

b) M32

The model for M32 is shown in figure 2b. The distribution of light and mass between the branches is very similar to that of M31 discussed above. In particular, the giant branch is stronger here than in any other elliptical in this work. The main sequence turnoff, at middle G, is the earliest of any galaxy here. This turnoff corresponds to an age of $6 \pm 1 \times 10^9$ years. The M/L for the model is 19±6. The fraction of SMR stars is lower than in M31, yet there is no trouble fitting the Mg and Na lines in M32. Thus there is no necessity for an abnormally high metal abundance in the nucleus of this galaxy.

The present model is again similar to the Spinrad and Taylor model, but older and containing more giants. Faber's model for M32 has fewer giants and higher M/L than the present model. The present model predicts a C-K color redder than that measured by Penston (1973). If the giant branch is taken to terminate at middle M rather than late M, the predicted color would agree well with the infrared measurement.

c) M81

The model for M81, shown in figure 2c, has somewhat less giant light and more metal poor light than the M31 model discussed above. The slope of the giant branch in M81 is steeper than in M31, and significantly fewer SMR giants are used. Furthermore, the residuals of the sodium and mag-

TABLE 6

POPULATION MODELS FOR THE GALAXIES

Parameter	Sigma	Our Galaxy	NGC 3031 (M81)	NGC 3115	NGC 3379	NGC 4473	NGC 4594 (M104)	NGC 5194 (M51)	NGC 221 (M32)	NGC 224 (M31)	NGC 584	NGC 1052
% RESIDUAL	...	...	4.80	4.68	5.22	4.51	5.58	4.36	3.18	4.48	5.46	7.22
	2	...	65.10	73.36	50.91	51.62	58.24	73.31	73.08	39.33	67.91	53.93
P1	1	...	54.25	69.87	48.49	49.16	55.47	73.31	49.47	37.45	64.68	51.37
UPPER MAIN	0	4.62	45.21	66.54	46.18	46.82	52.83	69.82	47.11	35.67	61.60	48.92
SEQUENCE SLOPE	1	...	37.67	63.37	43.98	44.59	50.31	66.50	44.87	33.97	58.67	46.59
	2	...	31.40	60.35	41.89	42.47	47.92	63.33	7.38	32.35	55.87	44.37
	2	...	5.19	5.42	4.83	5.48	5.67	1.68	4.82	5.02	5.36	6.14
P2	1	...	5.16	5.16	5.60	5.22	5.39	1.60	4.17	4.78	5.11	5.84
LOWER MAIN	0	2.21	4.29	4.92	4.38	4.97	5.13	1.52	3.97	4.56	4.86	5.57
SEQUENCE SLOPE	1	...	3.90	4.68	4.17	4.73	4.89	1.45	3.80	4.34	4.63	5.30
	2	...	3.55	4.50	3.97	4.51	4.65	1.38	0.34	4.13	4.41	5.05
	2	...	0.93	0.91	1.00	0.91	0.87	0.90	1.06	0.96	0.71	0.82
P3	1	...	0.89	0.86	0.95	0.87	0.83	0.85	1.01	0.91	0.68	0.78
MAIN SEQUENCE	0	1.15	0.85	0.82	0.91	0.83	0.79	0.81	0.96	0.87	0.64	0.75
TURNOFF	1	...	0.81	0.78	0.87	0.79	0.75	0.77	0.91	0.83	0.61	0.71
	2	...	0.77	0.75	0.83	0.75	0.72	0.74	0.83	0.79	0.58	0.68

TABLE 6 (CONT.)

POPULATION MODELS FOR THE GALAXIES

Parameter	Sigma	Our Galaxy	NGC 3031 (M81)	NGC 3115	NGC 3379	NGC 4473	NGC 4594 (M104)	NGC 5194 (M51)	NGC 221 (M32)	NGC 224 (M31)	NGC 584	NGC 1052
	2	...	0.74	0.74	0.67	0.67	0.67	0.67	4.72	0.67	0.73	0.45
P4	1	...	0.67	0.70	0.64	0.64	0.64	0.64	0.64	0.64	0.69	0.43
SUBGIANT-MAIN	0	...	0.61	0.67	0.61	0.61	0.61	0.61	0.61	0.61	0.66	0.41
SEQUENCE RATIO	1	...	0.55	0.64	0.58	0.58	0.58	0.58	0.58	0.58	0.63	0.39
	2	...	0.50	0.61	0.55	0.55	0.55	0.55	0.05	0.55	0.60	0.37
	2	...	4.98	3.55	3.92	4.17	3.46	3.70	4.06	3.64	4.73	3.56
P5	1	...	4.53	3.38	3.73	3.97	3.29	3.53	3.18	3.47	4.50	3.39
EVOLVED STAR	0	2.14	4.12	3.22	3.55	3.78	3.13	3.36	3.03	3.30	4.29	3.23
SLOPE	1	...	3.74	3.06	3.38	3.60	2.98	3.20	2.88	3.14	4.08	3.08
	2	...	3.40	2.92	3.22	3.43	2.84	3.05	2.49	2.99	3.89	2.93
	2	...	0.33	0.12	0.11	0.16	0.12	0.11	0.49	0.27	1.08	0.21
P6	1	...	0.30	0.12	0.10	0.15	0.12	0.10	0.26	0.26	1.02	0.20
GIANT-MAIN	0	0.03	0.27	0.11	0.10	0.14	0.11	0.10	0.25	0.25	0.98	0.19
SEQUENCE RATIO	1	...	0.25	0.11	0.09	0.14	0.11	0.10	0.24	0.24	0.93	0.18
	2	...	0.22	0.10	0.09	0.13	0.10	0.09	0.12	0.23	0.89	0.18

TABLE 6 (CONT.)

POPULATION MODELS FOR THE GALAXIES

Parameter	Sigma	Our Galaxy	NGC 3031 (M81)	NGC 3115	NGC 3379	NGC 4473	NGC 4594 (M104)	NGC 5194 (M51)	NGC 221 (M32)	NGC 224 (M31)	NGC 584	NGC 1052
P7 SMR FRACTION	2	...	0.66	0.74	0.76	0.76	0.76	0.76	1.00	0.86	0.11	0.76
	1	...	0.60	0.70	0.72	0.72	0.72	0.72	0.77	0.82	0.10	0.72
	0	0.10	0.55	0.67	0.69	0.69	0.69	0.69	0.73	0.78	0.10	0.69
	1	...	0.50	0.64	0.65	0.65	0.65	0.65	0.70	0.75	0.09	0.65
	2	...	0.45	0.60	0.62	0.62	0.62	0.62	0.06	0.71	0.09	0.62
P8 METAL POOR STARS	2	...	1.06	1.65	1.24	1.61	1.38	1.85	1.76	0.98	2.17	1.48
	1	...	0.96	1.57	1.18	1.54	1.31	1.76	1.19	0.93	2.07	1.41
	0	0.001	0.87	1.49	1.12	1.46	1.25	1.68	1.13	0.88	1.97	1.35
	1	...	0.79	1.42	1.07	1.39	1.19	1.60	1.08	0.85	1.88	1.28
	2	...	0.72	1.35	1.02	1.33	1.13	1.52	0.60	0.81	1.79	1.22
M/L RATIO	2	...	122.4	127.4	101.0	146.8	154.3	1.3	70.4	89.3	31.5	207.9
	1	...	66.1	92.1	74.2	107.0	112.4	1.2	25.8	64.3	22.7	153.1
	0	...	36.1	66.4	54.5	77.4	81.2	1.2	18.9	46.4	16.6	110.9
	1	...	20.5	48.0	40.3	56.1	58.7	1.1	14.1	33.8	12.4	79.8
	2	...	12.3	35.0	30.1	40.9	42.6	1.0	0.6	24.8	9.4	57.5

Figure 2

Parameterized population models for the ten galaxies. The points are the optimal parameterized model, the inner pair of solid lines the one standard deviation limits, the outer pair the two standard deviation limits. (a) M31, (b) M32, (c) M81, (d) M51, (e) M104, (f) NGC 3115, (g) NGC 3379, (h) NGC 4473, (i) NGC 1052, and (j) NGC 584.

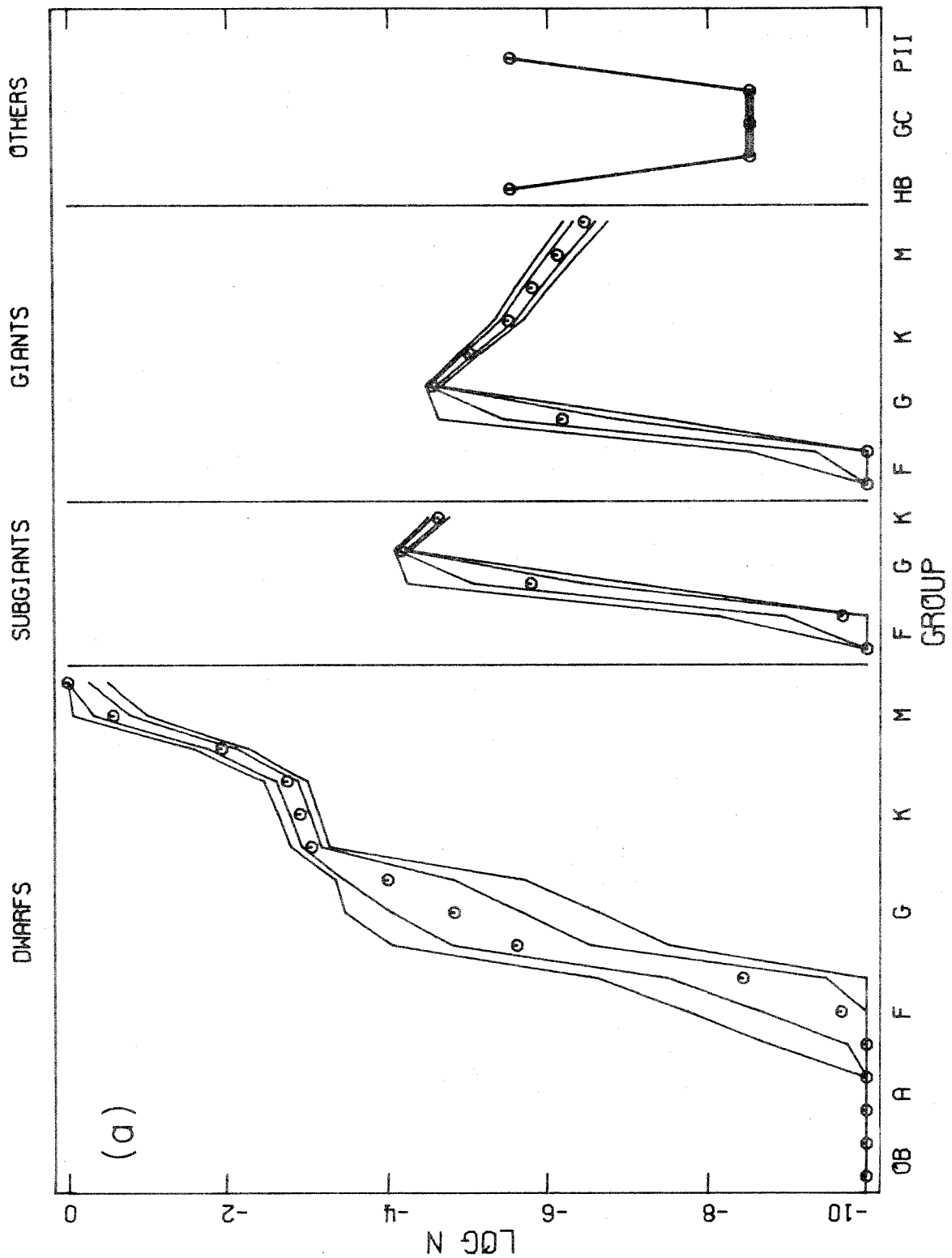
DWARFS
SUBGIANTS
GIANTS
OTHERS
(a)
LOG N
0
-2
-4
-6
-8
-10
OB A F G K M F G K F G K M HB GC PII
GROUP

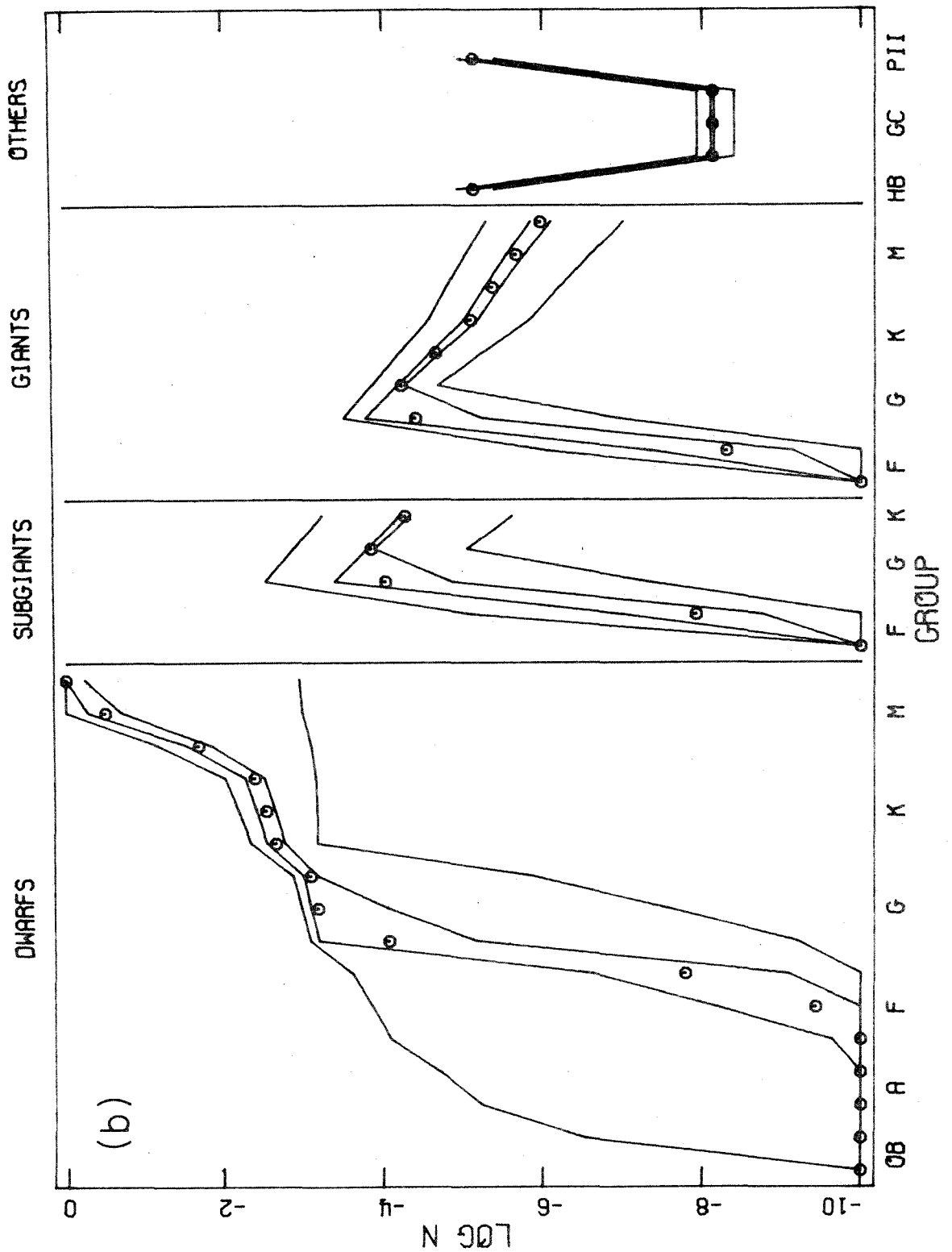
DWARFS
SUBGIANTS
GIANTS
OTHERS
(b)
LOG N
0
-2
-4
-6
-8
-10
OB A F G K M F G K F G K M HB GC PII
GROUP

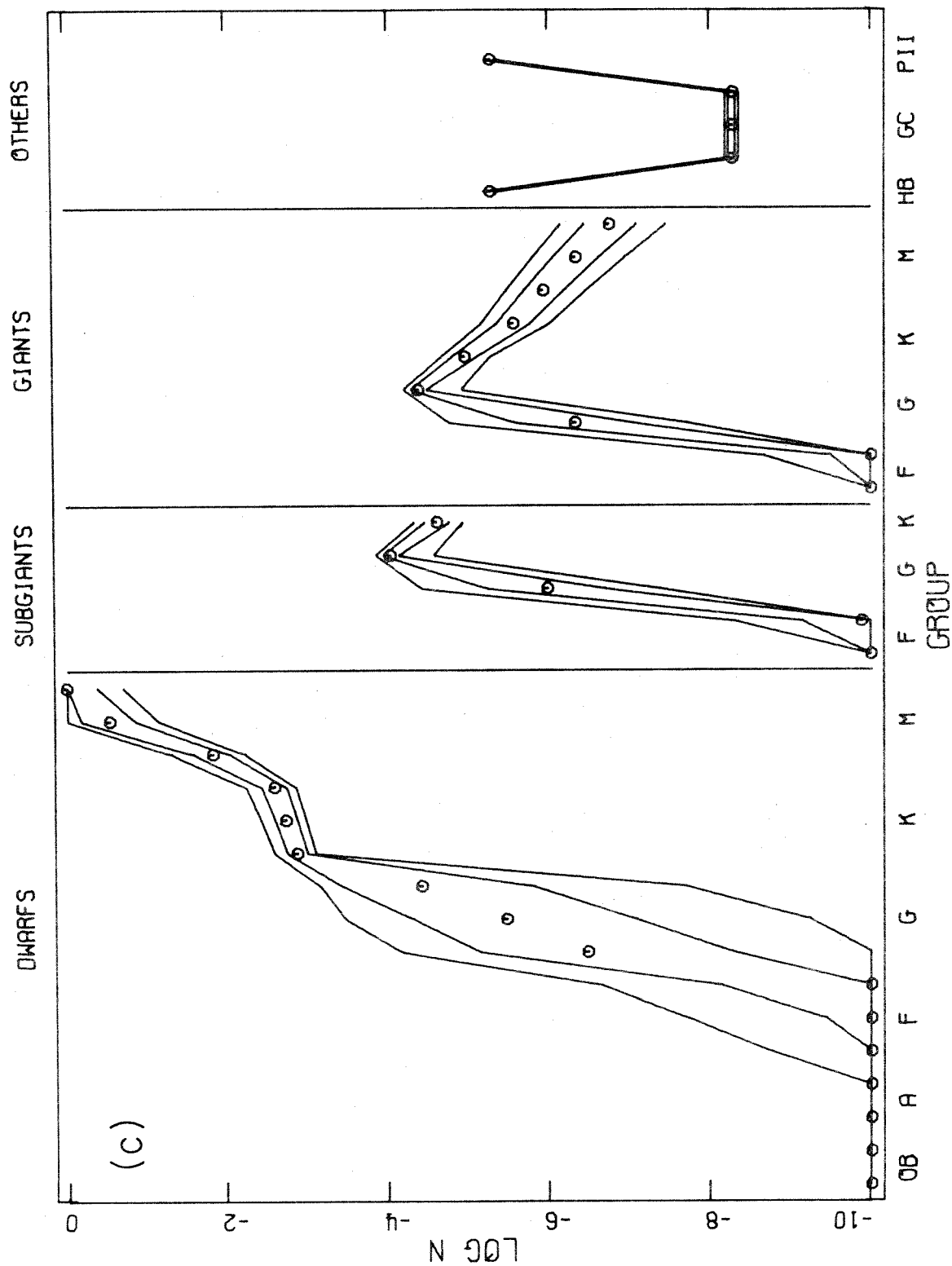
DWARFS
SUBGIANTS
GIANTS
OTHERS
(C)
LOG N
0
-2
-4
-6
-8
-10
OB A F G K M F G K F G K M HB GC PII
GROUP

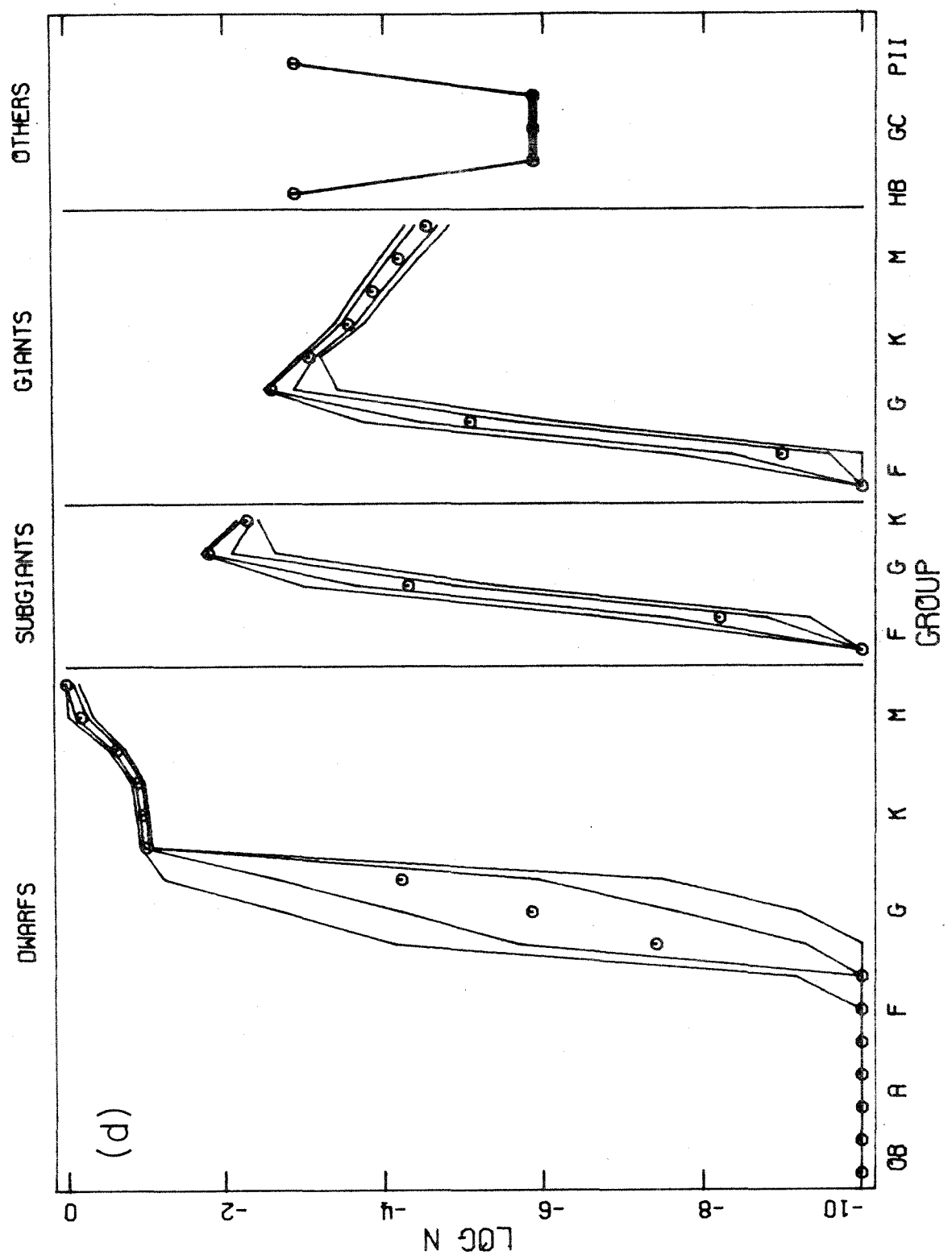
DWARFS
SUBGIANTS
GIANTS
OTHERS
(d)
LOG N
0
-2
-4
-6
-8
-10
OB A F G K M F G K M F G K M HB GC PII
GROUP

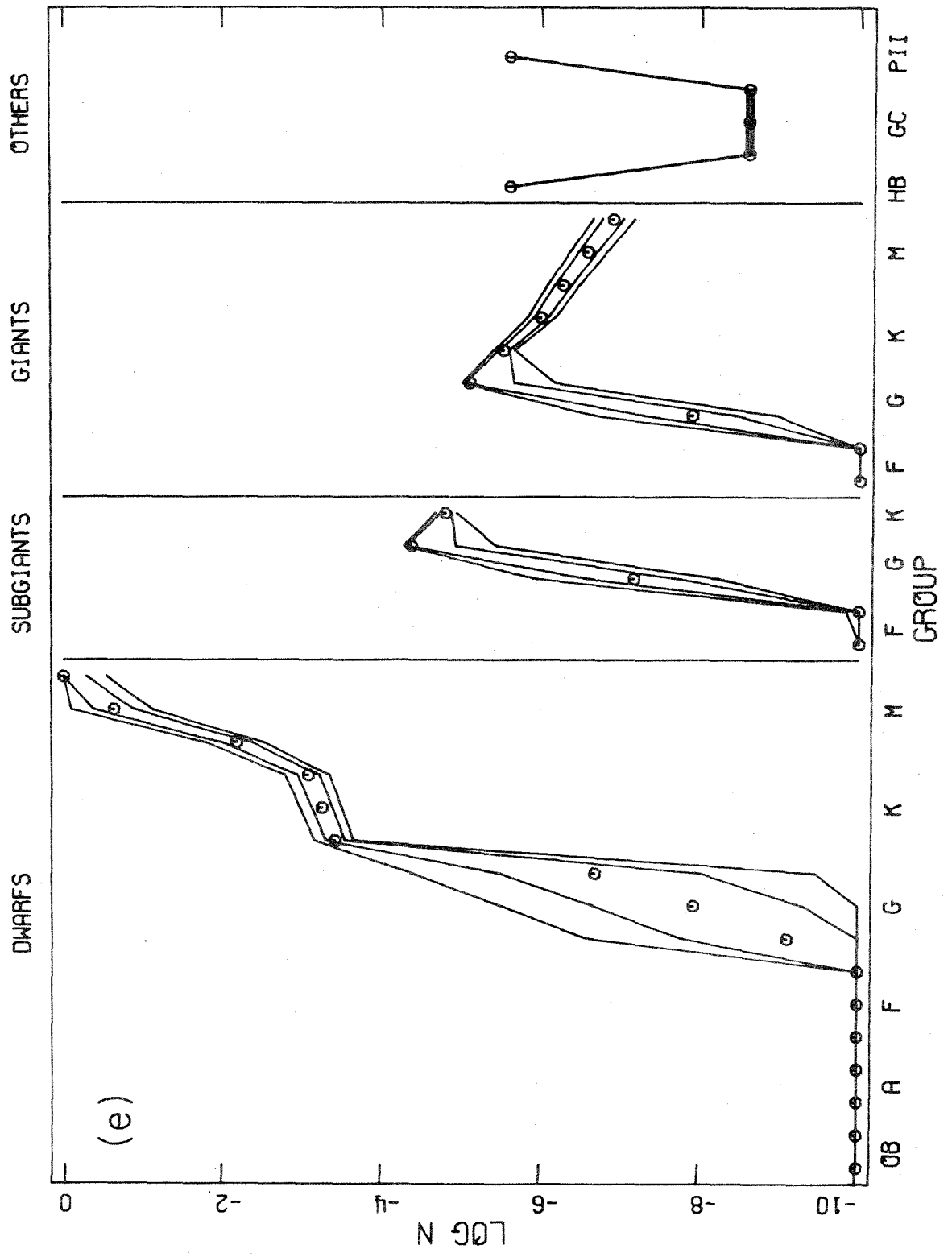
DWARFS
SUBGIANTS
GIANTS
OTHERS
(e)
LOG N
0
-2
-4
-6
-8
-10
OB A F G K M F G K M F G K M HB GC PII
GROUP

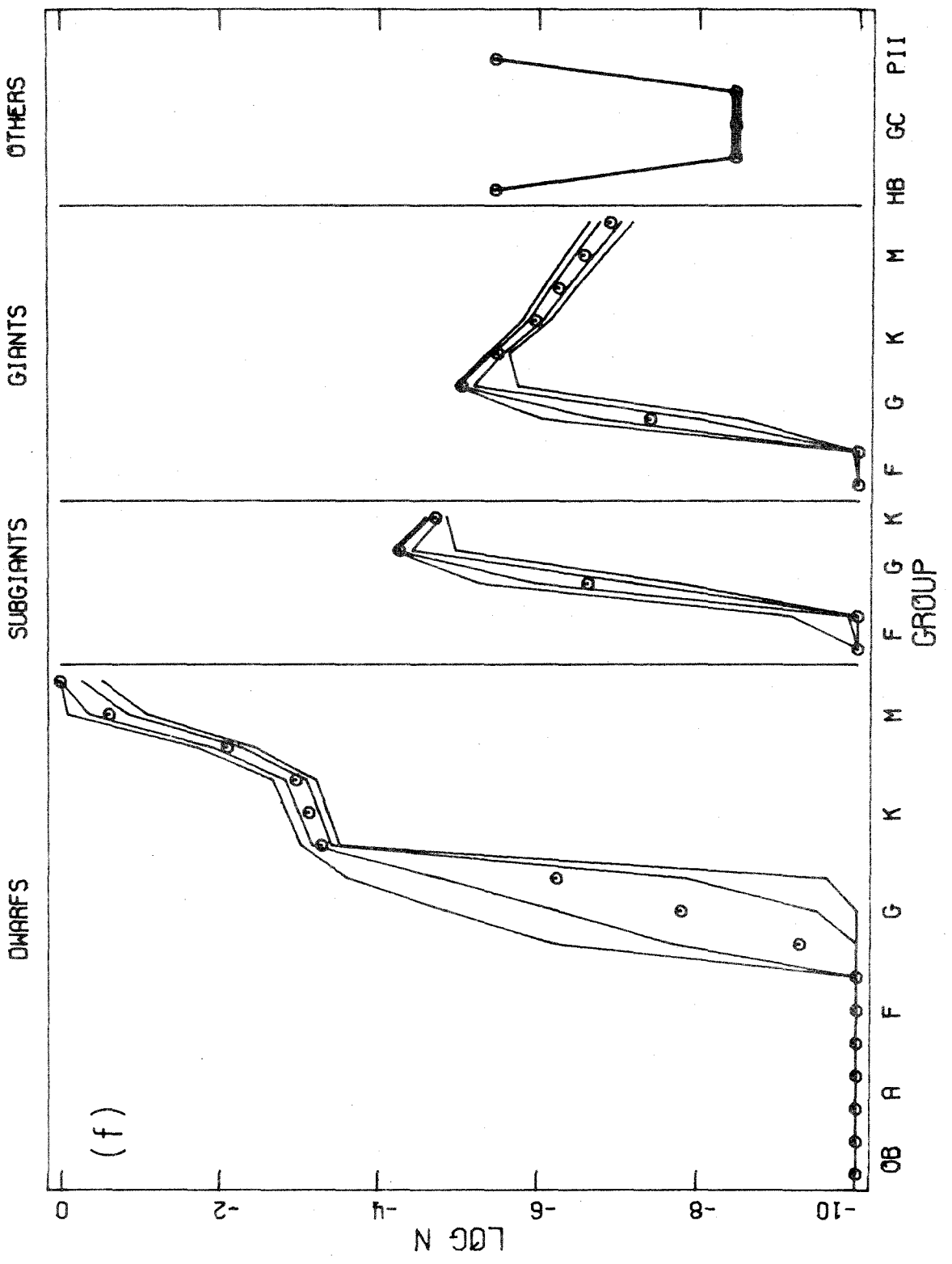
DWARFS
SUBGIANTS
GIANTS
OTHERS
(f)
LOG N
0
-2
-4
-6
-8
-10
OB A F G K M F G K M F G K M HB GC PII
GROUP

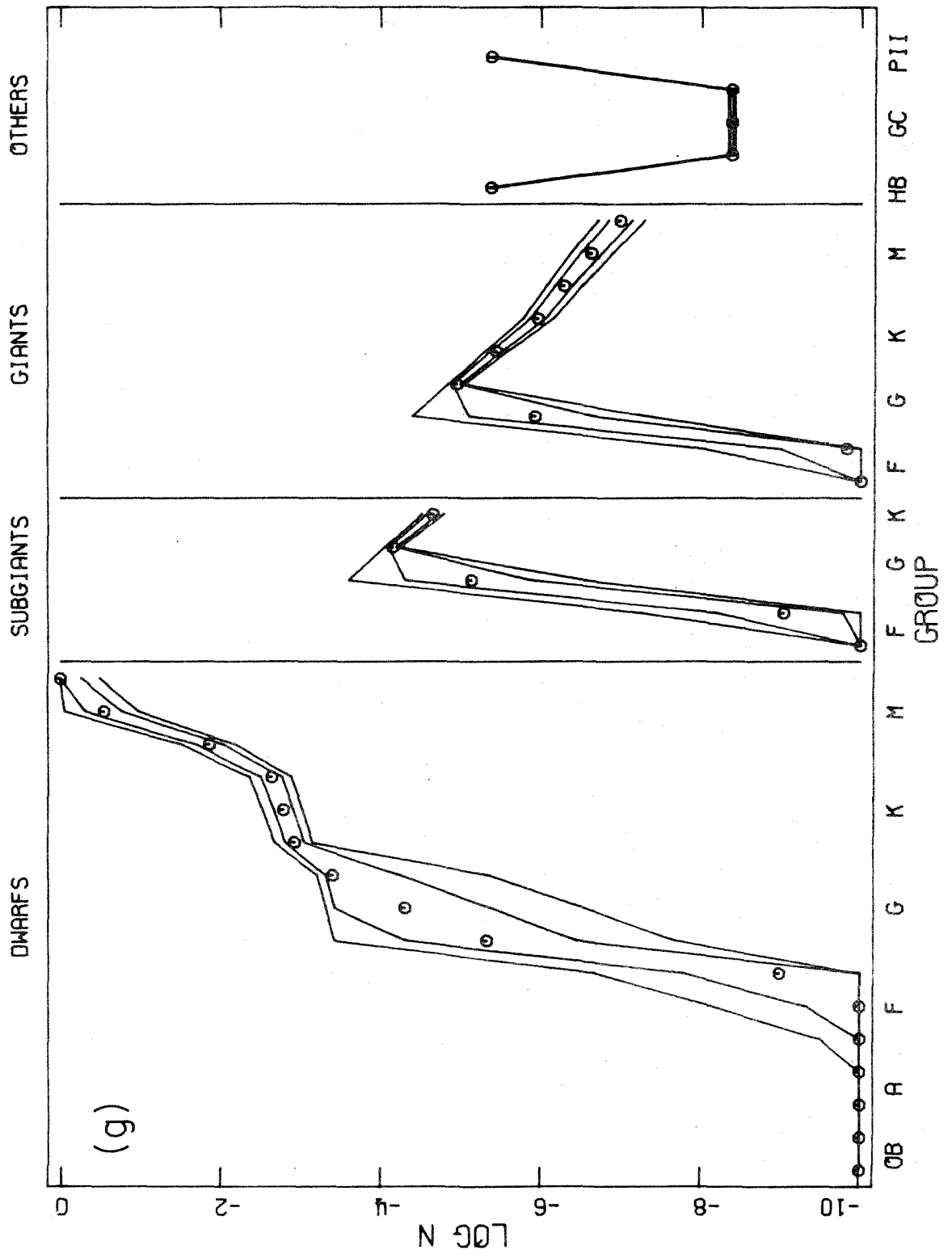
DWARFS
SUBGIANTS
GIANTS
OTHERS
(g)
LOG N
0
-2
-4
-6
-8
-10
OB A F G K M F G K M K G F M HB GC PII
GROUP

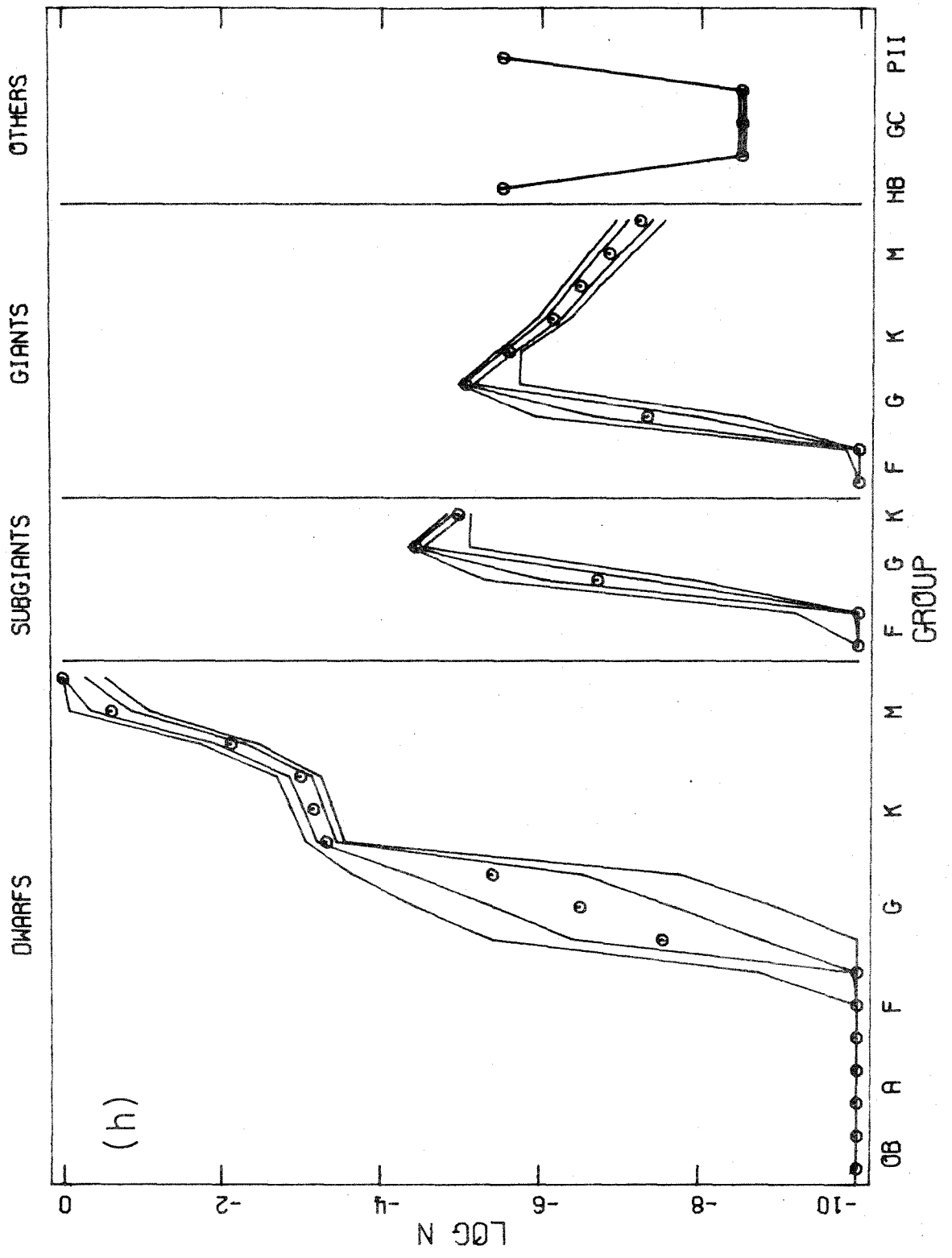
DWARFS
SUBGIANTS
GIANTS
OTHERS
(h)
LOG N
0
-2
-4
-6
-8
-10
OB A F G K M F G K F G K M HB GC PII
GROUP

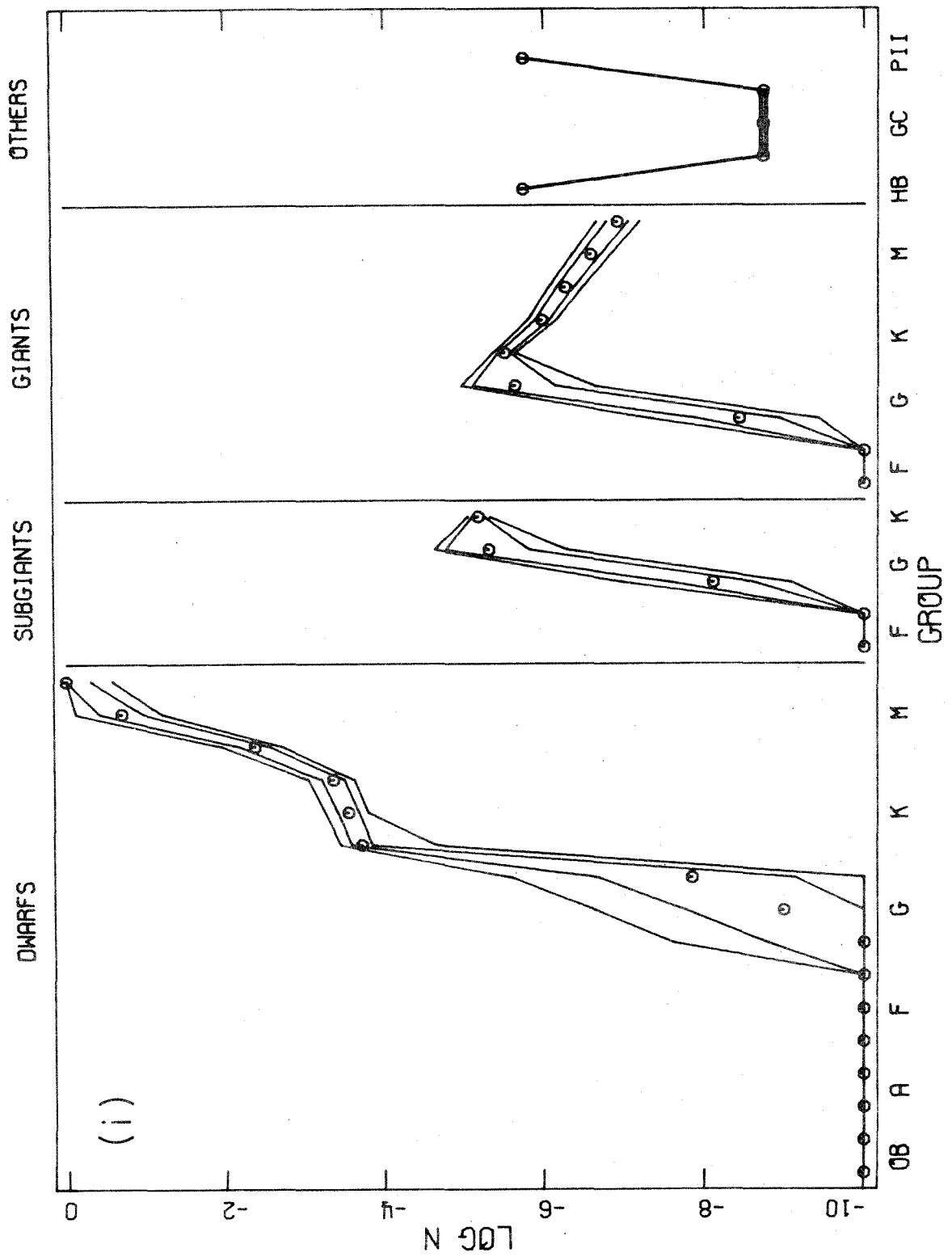
DWARFS
SUBGIANTS
GIANTS
OTHERS
(i)
LOG N
0
-2
-4
-6
-8
-10
OB A F G K M F G K M G K M HB GC PII
GROUP

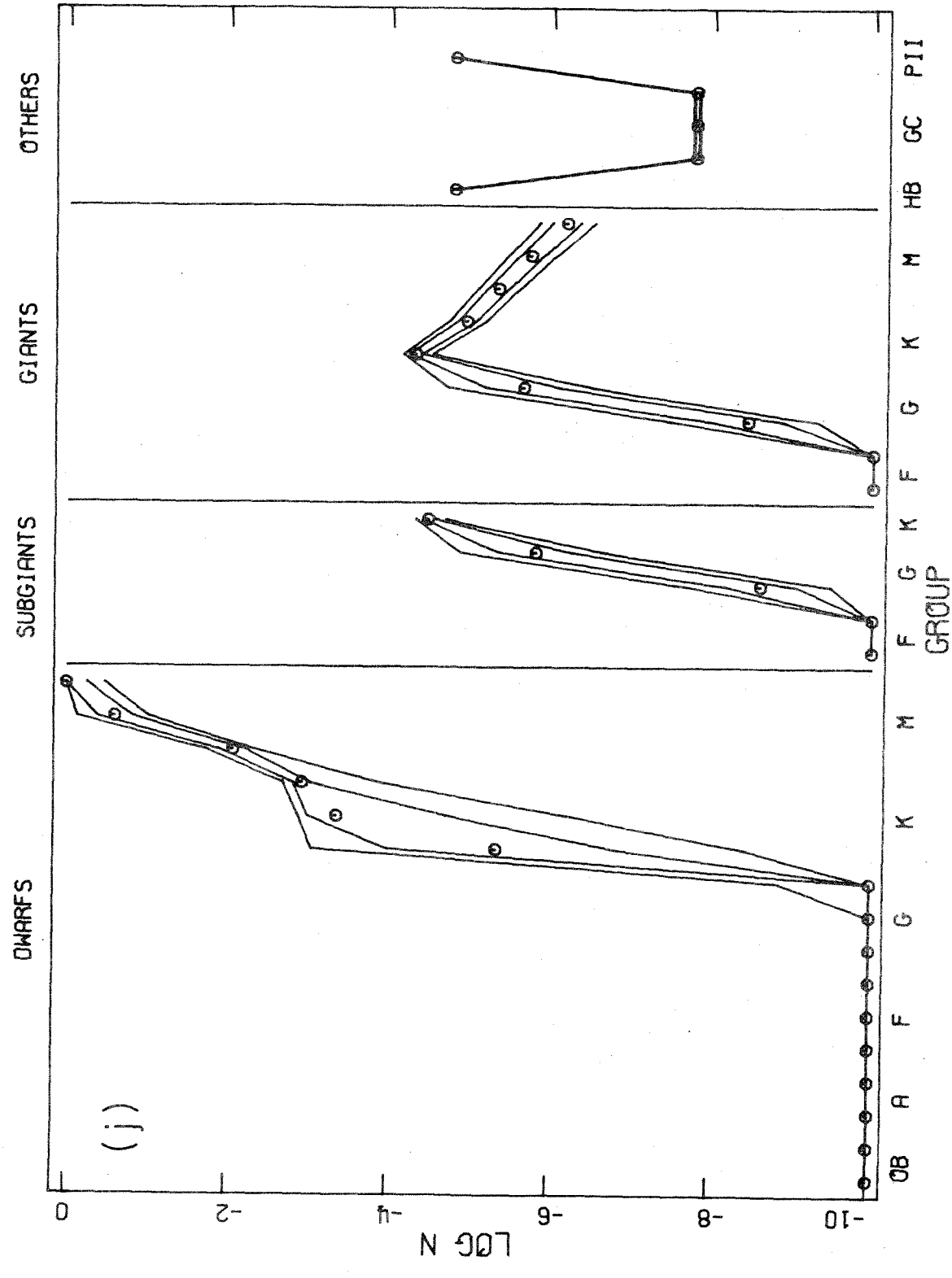
DWARFS
SUBGIANTS
GIANTS
OTHERS
(i)
LOG N
0
-2
-4
-6
-8
-10
OB A F G K M F G K M F G K M HB GC PII
GROUP

nesium lines are within the observational errors, suggesting less metal enhancement in this galaxy. The M/L is 36±25, and the turnoff age 8.5 ±1.5 billion years.

The models of M81 produced by Spinrad and Taylor and by Faber are very different from this model. Theirs contain a strong giant branch with 77 percent of the light, an earlier turnoff, lower mass-to-light ratio, and no metal poor stars. Their models do find the metallicity of the giants and the slope of the lower main sequence similar to the present model. None of the models are able to produce the CO index observed by Baldwin, et al.

d) M51

The model for M51, in figure 2d, is totally different from all the other galaxies in this study. It has a very flat lower main sequence which contributes only 3 percent of the light and 58 percent of the mass. The strongest light contribution comes from metal poor stars, with 66 percent; the evolved branches have 31 percent of the light. The flat lower main sequence produces a very low M/L of 1.2±0.1. The turnoff is late, between late G and early K, with a corresponding age of 10 ±2 billion years.

This unusual model is caused by the relatively strong hydrogen and other early type lines, and relatively weak late type lines, as seen in Table 5.

A model of M51 by Turnrose (1975) has a main sequence turnoff, mass-to-light ratio, and shape of the lower main sequence which are similar to the present model. His observations include no metal poor stars, thus his model has a substantially populated upper main sequence which contributes light similar to that which the present model derives from metal poor stars. Indeed, if no metal poor stars are allowed, my procedure requires many more upper main sequence stars, but the goodness of fit is significantly lower. Thus we believe that the early type absorption lines in the spectrum of M51 are probably coming from metal poor stars.

e) M104

For this and subsequent galaxies in this study, there exist no previously published models by other investigators. The model for M104 is shown in figure 2e. The main sequence has 22 percent of the V light, and 99 percent of the mass. The evolved stars have 34 percent of the light, and the metal poor stars, 43 percent. The M/L is 81 ± 25, and the turnoff at early K, or 11 ±2 billion years. In most respects, the nucleus of this Sa galaxy seems more like the ellipticals discussed below than the spirals discussed above.

f) NGC 3115

The NGC 3115 model is shown in figure 2f. The main sequence has 20 percent of the light, the evolved stars 31 percent, and the metal poor stars 49 percent. The turnoff is at late G, with corresponding age 9.5 ±1.5 billion years. The M/L is 66±30. Morton and Chevalier (1973) found an M/L of 38 for the nucleus of this galaxy from its velocity dispersion; this value is within the uncertainties of the M/L from the synthesis model.

g) NGC 3379

The model for this E1 galaxy is shown in figure 2g. The distribution of light between the components of the model is similar to that of M104 above. The turnoff is much earlier, however, at mid-G, with an age of 6.5 ±1 billion years. The M/L is 55±20.

h) NGC 4473

Figure 2h shows the model for NGC 4473. The light and mass distribution is again similar to M104. The M/L is 77±25. The turnoff is at late G, or 9 ±1.5 billion years.

i) NGC 1052

The model for this galaxy is shown in figure 2i. The light distribution is again similar to that of M104. The M/L is 111±40, and the turnoff at early K gives an age of

13 ±2 billion years. This is the only galaxy besides M31 which shows evidence of metal enrichment in the nucleus. The magnesium and sodium lines of the model are significantly too weak and cannot be brought into agreement with observations by any value of the metallicity parameter.

j) NGC 584

The model of this elliptical is in figure 2j. The model is distinctly different from the rest of the ellipticals in the survey. The main sequence has only 4 percent of the light, the subgiants less than 1 percent, the giants 38 percent, and metal poor stars 57 percent. The most striking feature is the late turnoff, at mid K, corresponding to an age of 23 ±4 billion years. The metallicity parameter is approximately a tenth that of the other galaxies, and the metal poor star contribution is the strongest of all the models in this work. The ratio of giants to main sequence is high, giving a mass-to-light ratio of 17 ±5. The overall impression is that of an extremely old stellar population. This old population model is caused by the relatively strong molecular bands and relatively weak early type lines, as seen in Table 5.

VII. SYSTEMATIC PROPERTIES OF THE MODELS

a) Metallicity

In general, most of the galaxies observed show no evidence of requiring stars of higher metal content than those observed in the solar neighborhood. Only M31 and NGC 1052 appear to be highly metal enriched, and the result for the latter galaxy is tentative, since its model has significantly poorer overall residuals than the others in this study. Most of the models use approximately 70 percent solar neighborhood SMR stars and 30 percent normal stars; NGC 584 uses normal abundance stars almost exclusively. Metal poor stars contribute significantly to all models, with about half the light of ellipticals and a quarter the light of Sb galaxies.

b) Evolved Stars

Most of the models have significant light contributions from M giant stars, often equal to or greater than the light from the M dwarfs. The presence of these M giants predicts infrared colors in better agreement with observations than those deduced from previous models. The evolved stars contribute approximately twice as much light to the models of Sb galaxies as to the elliptical galaxy models.

c) Population Age

From the position of the main sequence turnoff, the

spirals appear to have had star formation occurring in their nuclei as recently as 8 billion years ago. Surprisingly, two of the ellipticals seem to have had star formation more recently than this, and in another elliptical, at 9 billion years. The two young ellipticals are very close to spiral galaxies, and the third is near the center of the Virgo cluster. It is thus reasonable to assume that these galaxies have had infall of gas from their spiral companions, which has triggered recent star formation. The other two ellipticals, which have ages on the order of or greater than the Hubble time, are more nearly isolated. Similar suggestions of gas infall have been advanced by van den Bergh (1975). If the gas in these ellipticals has not come from spiral companions, but from some intergalactic medium, a theory must be advanced which explains why some of the ellipticals show no evidence of such infall.

d) Morphological Type

The models described above reveal differences in stellar population which correlate with morphological type. The ellipticals have more metal poor stars and fewer evolved stars than later type galaxies. The principal difference among the ellipticals seems to be the degree to which they have interacted with nearby galaxies. NGC 584 appears to have a very old population and has probably evolved since

its formation without interaction with any other galaxies; M32, with the youngest population of this study, has undoubtedly interacted strongly with M31 in the past. The S0 and Sa galaxies studied here seem to be more like the ellipticals than the later type spirals. The Sb galaxies have more giants, fewer metal poor stars, and perhaps slightly more upper main sequence stars than the earlier type galaxies. The Sc galaxy similarly has an enhanced giant branch, but has a far flatter lower main sequence than any other galaxy in this survey. Thus the galaxies in this study can be divided by morphological type into three distinct population groups: E0 through Sa, Sb, and Sc.

VIII. CONCLUSIONS

The stellar populations of galaxies can be synthesized from their composite spectra, using the techniques described above. The resulting models are both astrophysically reasonable and consistent with previous investigations. The high spectral resolution of the data in this study is an important improvement over earlier work. For example, this high resolution increases the sensitivity to luminosity indicators in the late type stars. The resulting models predict infrared colors for the galaxies more nearly in accord with observations than earlier models, even though the observations of this work extend only to 6800 Å.

Future observational work on this subject should concentrate on both high spectral resolution and photometric measurements of color. The new generation of high resolution, high sensitivity, linear detectors now being developed should be ideal for such a study. Further work remains to be done on the method of synthesis. Different schemes of parameterization should be investigated, both to determine the sensitivity of the results to the form of parameterization, and to find a form which is more flexible yet insensitive to noise in the data.

The author would like to thank Dr. J. E. Gunn and B. Turnrose for kindly providing data in advance of publication. E. Turner furnished the velocity-finding algorithm and much helpful advice in the course of this work. Dr. J. Gunn constructed the wedge calibrator and kindly allowed me to use it. L. Blakee, M. Olsiewski, and O. Smith maintained the electronic equipment. The author was supported during part of this work by a National Science Foundation pre-doctoral fellowship.

APPENDIX

An Algorithm for Locating Spectral Lines in Digital Spectra

The first step of the procedure to find emission and absorption lines in digitized spectra is to locate the continuum level. A data window is chosen whose width is less than the average spacing between spectral lines. This window is moved along the spectrum in steps which are a tenth of the window's width; at each step, the mean and standard deviation of the data within the window are estimated. When there are no spectral lines in the window, the mean is the continuum level at that point, and the standard deviation gives an estimate of the noise level there. If there are one or more lines in the window, the standard deviation of that point is much larger than the deviation of the line free points. After the entire spectrum is scanned in this manner, a low order polynomial is passed through the mean values, weighting each mean by the inverse square of its standard deviation. This weighting causes the polynomial to pass through the continuum points and to essentially ignore the points contaminated by spectral lines. In an emission line spectrum, the polynomial lies slightly above the continuum, in an absorption line spectrum, slightly below.

After the continuum and its noise level have been

estimated, the spectrum is examined point by point. All features more than a given number of standard deviations from the continuum are considered to be lines. The peak of each line is found, and a parabola is fit to the upper half of the line. The center of the parabola is taken to be the line position, and the error of the position is estimated from the dispersion in the fit. If multiple peaks are found in partially blended lines, each peak is fit as described above. If a line is single-peaked but asymmetric due to more severe blending, the error estimate will be appropriately larger, reflecting the asymmetry.

REFERENCES

Baldwin, J. R., Danziger, I. J., Frogel, J. A., and Persson, S. E. 1973, Ap. Letters, 14, 1.

Blaauw, A. 1963, in Basic Astronomical Data, Ed. K. Aa. Strand (Chicago: University of Chicago Press), p. 383.

———. 1965, in Galactic Structure, Ed. D. Blaauw and M. Schmidt (Chicago: University of Chicago Press), p. 435.

———. 1973, Ed. B. Hauck and B. E. Westerlund, I.A.U. Symp. No. 54, 47.

Christensen, C. G. 1972, Ph.D. Thesis, California Institute of Technology.

de Vaucouleurs, G. 1967, Publ. Dept. Astron., Univ. Texas, (II), No. 3.

de Vaucouleurs, G., and de Vaucouleurs, A. 1964, Reference Catalogue of Bright Galaxies (Austin: University of Texas Press).

Faber, S. M. 1972, Astr. and Ap., 20, 361.

Gahm, G. F. 1970, Astr. and Ap., 4, 279.

Gahm, G. F., and Hultquist, L. 1972, Astr. and Ap., 16, 329.

Gliese, W. 1969, Catalogue of Nearby Stars, Veröff. Astr. Rechen-Inst. Heidelberg, No. 22.

Harris, D. L. III, Strand, K. Aa., and Worley, C. E. 1963, in Basic Astronomical Data, ed. K. Aa. Strand (Chicago: University of Chicago Press) p. 273.

Jaschek, C., Conde, H., and de Sierra, A. C. 1964, Catalogue of Stellar Spectra Classified in the Morgan-Keenan System, Obs. Astron. Univ. la Plata, No. 28.

Jolly, M. 1974, Astr. and Ap., 33, 177.

Jolly, M., and Andrillat, Y. 1973, Astr. and Ap., 26, 95.

Keenan, P. C. 1963, in Basic Astronomical Data, ed. K. Aa. Strand (Chicago: University of Chicago Press), p. 78.

Moore, J. H., and Paddock, G. F. 1950, Ap. J., 112, 48.

Morgan, W. W., Keenan, P. C., and Kellerman, E. 1943, An Atlas of Stellar Spectra (Chicago: University of Chicago Press).

Morgan, W. W., and Mayall, N. U. 1957, PASP, 69, 291.

Morton, D. C., and Chevalier, R. A. 1973, Ap. J., 179, 55.

O'Connell, R. F. 1970, Ph.D. Thesis, California Institute of Technology.

Penston, M. V. 1973, M.N.R.A.S., 162, 359.

Rood, R. 1972, Ap. J., 177, 681.

Sandage, A. R. 1961, The Hubble Atlas of Galaxies, Carnegie Institution of Washington Pub. No. 618.

Spinrad, H., and Taylor, B. J. 1971, Ap. J. Suppl., 22, 445.

Strömgren, B. 1963, in Basic Astronomical Data, ed. K. Aa. Strand (Chicago: University of Chicago Press), p. 123.

Turner, E. L. 1976, Ph.D. Thesis, California Institute of Technology.

Turnrose, B. E. 1975, Ph.D. Thesis, California Institute of Technology.

van den Bergh, S. 1975, Ann. Rev. Astr. and Ap., 13, 217.

Veeder, G. J. 1974, Ph.D. Thesis, California Institute of Technology.

Vyssotsky, A. N. 1963, in Basic Astronomical Data, ed. K. Aa. Strand (Chicago: University of Chicago Press), p. 192.

Williams, T. B. 1976a, Ap. J. (Letters), in publication.

————. 1976b, Ap. J., in preparation.

CHAPTER 3

VELOCITY DISPERSIONS IN THE NUCLEI OF TEN NEARBY GALAXIES

I. INTRODUCTION

The measurement of the velocity dispersion of the stars in the center of elliptical galaxies is important, for it provides an estimate of the mass of the galaxy, and a clue to the processes by which the galaxy formed. In addition, Faber and Jackson (1975) have suggested that velocity dispersion is correlated with luminosity for normal ellipticals. The velocity dispersion at the nucleus of a spiral galaxy similarly provides a measure of the mass of the central part of the spheroidal bulge component of these systems. Thus it is important to obtain reliable estimates of the velocity dispersions of all types of regular galaxies.

The first investigations of velocity dispersion were performed by Minkowski (1962), who compared photographic spectra of galaxies with stellar spectra broadened in an analogue fashion. Burbidge, Burbidge and Fish (1961a,b), de Vaucouleurs (1974) and Richstone and Sargent (1972) have used digital techniques to broaden the photographic spectra of stars and compare them with galaxy spectra. Morton and co-workers (1973) and Faber and Jackson (1975) have used linear photoelectric devices to obtain the spectra used to estimate velocity dispersions. All of these previous investigations have used for comparison single stars whose spectra appeared similar to those of the galaxy. However, galaxy spectra are composite, and thus

the match with the spectrum of any single star is only approximate. In the present investigation, composite spectra of standard stars, determined in a previous paper (Williams, 1976, hereafter Paper I), are used for comparison. This is the first time such composite spectra have been used, and this procedure leads to systematically lower estimates of the velocity dispersion.

Section II of this paper discusses briefly the observations, data reduction, and population synthesis procedures; a complete discussion of these matters is presented in Paper I. Section III describes the procedure for broadening the spectra, and presents the results for both composite spectra and for single star spectra. Section IV derives mass to light ratios for the galaxies in this study. Section V summarizes our results.

II. OBSERVATIONS, DATA REDUCTION, AND SYNTHESIS

All spectra were obtained with the Palomar 1.5 m telescope, using the two-stage image-tube spectrograph. The spectra extend from 3800 Å to 6800 Å, at dispersions of 40 Å mm^{-1} in the blue and 60 Å mm^{-1} in the red, with resolution of 2 Å. Ten galaxies, 137 stars, and 5 globular clusters were observed. For the galaxies, the slit was 15 arc seconds long, and oriented perpendicular to the plane of each galaxy to minimize the effects of rotation. The spectra were measured with a digital microphotometer, corrected for the nonlinear film response, shifted to zero velocity, and corrected for the geometric distortions of the image tube. Comparison of the spectra with photoelectric scans of standard stars suggests that the total photometric errors are less than 5% in these spectroscopic data.

Line indices were measured for 74 absorption lines and bands in the spectra. The allowed distributions of stars in the models of the galaxies are described by an eight parameter power law representation. A computer algorithm finds that set of parameters which minimizes the RMS difference between the composite stellar indices and the observed galaxy indices. These optimal parameterized models are listed for each galaxy in Paper I. These optimal models provide the distribution of stars used to construct the composite spectra discussed below.

III. VELOCITY DISPERSIONS

To simplify the computation of the broadened spectrum, the composite synthesized spectrum was first transformed to a logarithmic wavelength scale so that:

$$\lambda_{i+1} = (1+f)\ \lambda_i$$

Here f was chosen to keep the number of samples in the logarithmic spectrum equal to the number of samples in the linear spectrum. This logarithmic spectrum was then broadened as follows:

$$S'(\lambda_i, \sigma) = A^{-1} \sum_j \exp\left\{ - \frac{c^2 (\lambda_j - \lambda_i)^2}{2\sigma^2 \lambda_i^2} \right\} S(\lambda_j)$$

$$= A^{-1} \sum_j \exp\left\{ - \frac{c^2 (j - i)^2 f^2}{2\sigma^2} \right\} S(\lambda_j)$$

Here S' is the broadened spectrum, S the composite spectrum, c the speed of light, σ the velocity dispersion, and A a normalization factor:

$$A = \sum_j \exp\left\{ - \frac{c^2 (j - i)^2 f^2}{2\sigma^2} \right\}$$

The summation extends over all values of j for which the exponential term is greater than or equal to 10^{-4}. After the entire spectrum is broadened in this manner, it is

transformed back to a linear wavelength scale.

The composite spectrum for each galaxy was broadened with several different velocity dispersions, and the spectrum with the best match to the actual galaxy spectrum was selected by visual inspection. The plots of the broadened spectra were identified with a code, so that the author did not know which galaxy nor which velocity dispersions were being inspected when the selection of best fit was made. Thus it is hoped that personal biases were avoided in the estimation of velocity dispersion. The velocity dispersions thus determined are listed in Table 1. We conservatively estimate the errors in these dispersions at 15%. Figure 1 shows the observed galaxy spectra and several broadened composite spectra near the best velocity dispersion for each galaxy. In Figure 1, the composite spectrum and the galaxy spectrum are separated vertically by a small amount to prevent serious overlapping of the curves; the arrow shows the amount of separation. The galaxy spectrum is always the lower of each pair. A third order polynomial is added to the composite spectrum to correct for differences in the continuum between the galaxy and the composite; this polynomial is shown below each pair, drawn to scale but with a zero point shift.

The velocity dispersions estimated from the composite spectra are systematically lower by 53 ±17 km sec^{-1}

TABLE 1

VELOCITY DISPERSIONS FOR THE TEN GALAXIES

Galaxy (NGC)	Type	Velocity Dispersions (km/sec^{-1}) This Paper		Other Works*					
		Composite Spectra	Single Stars	Mi	BBF	dV	Mo	FJ	RS
221	E2	55	...	100	96	60	...	<100	60
224	Sb	125	166	225	...	150	120	180	...
584	E4	150	...	...	...	...	...	...	...
1052	E4	100	...	...	...	...	...	...	...
3031	Sb	150	...	...	...	...	...	...	...
3115	E7-SO	200	240	205	...	230	215	300	...
3379	E1	133	225	...	187	125	...	240	...
4473	E5	110	200	...	...	...	160	...	...
4594	Sa	215	...	...	...	...	...	...	...
5194	Sc	75	...	...	...	...	...	...	...

*Key to References: Mi: Minkowski (1962), BBF: Burbidge et al. (1961a,1961b), dV: de Vaucouleurs (1974), FJ: Faber and Jackson (1975), RS: Richstone and Sargent (1972) Mo: 224: Morton and Thuan (1973); 3115, 4473: Morton and Chevalier (1973).

Figure 1

Velocity dispersions for the ten galaxies. The upper curve of each pair is the broadened composite stellar spectrum; the lower is the observed galaxy spectrum. The two spectra of each pair are separated a distance shown by the arrow. The smooth curve is a polynomial added to the composite spectrum to adjust its color to that of the galaxy; this curve is drawn to the same relative intensity scale as the spectra, but with a zero point shift - zero is the level at 4200 Å. The best velocity dispersion is shown in the central plot. (a) NGC 224, (b) NGC 221 (c) NGC 3031, (d) NGC 5194, (e) NGC 4594, (f) NGC 3115, (g) NGC 3379, (h) NGC 4473, (i) NGC 1052, and (j) NGC 584.

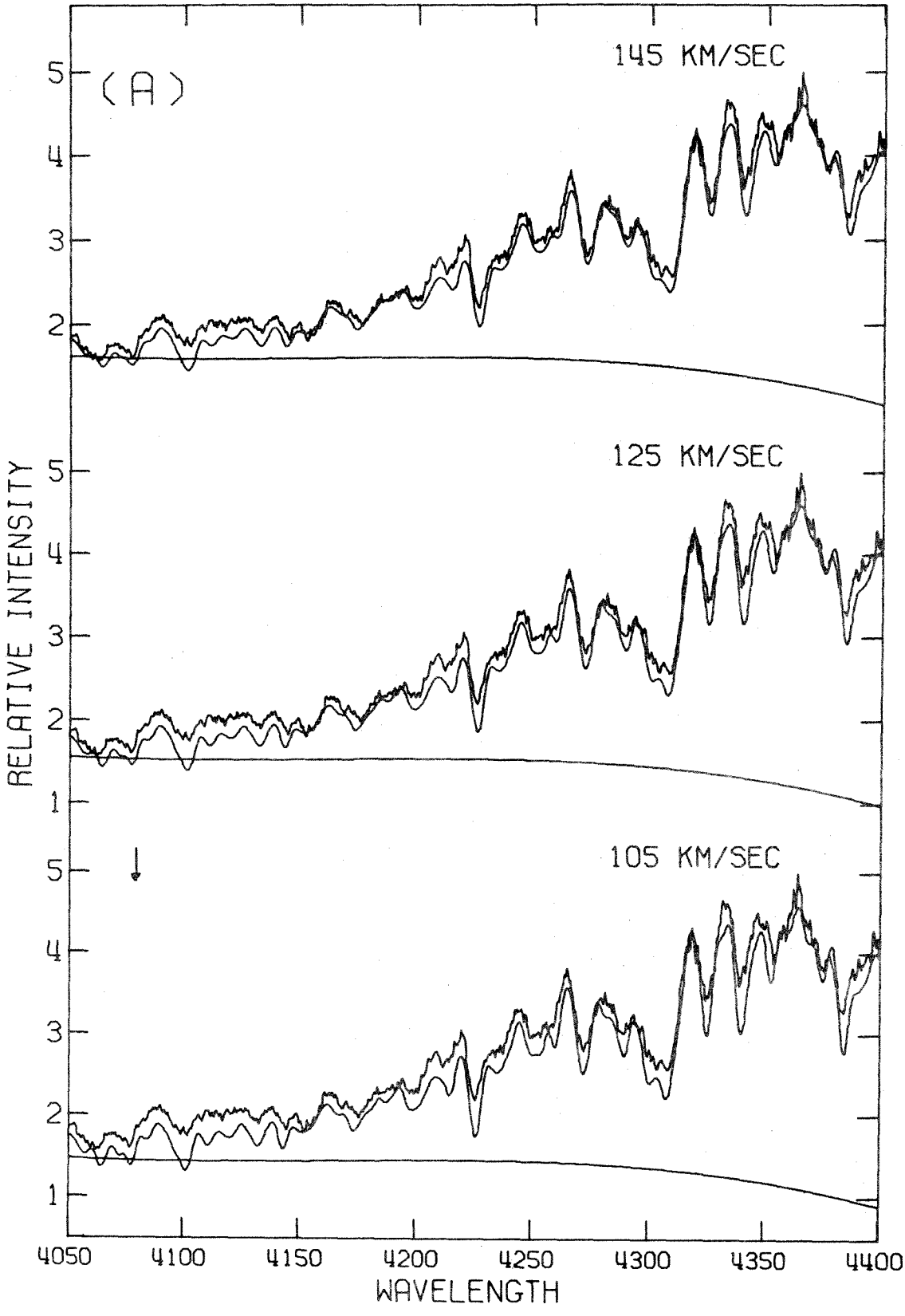
(A)
145 KM/SEC
125 KM/SEC
105 KM/SEC
RELATIVE INTENSITY
WAVELENGTH
4050
4100
4150
4200
4250
4300
4350
4400
1
2
3
4
5

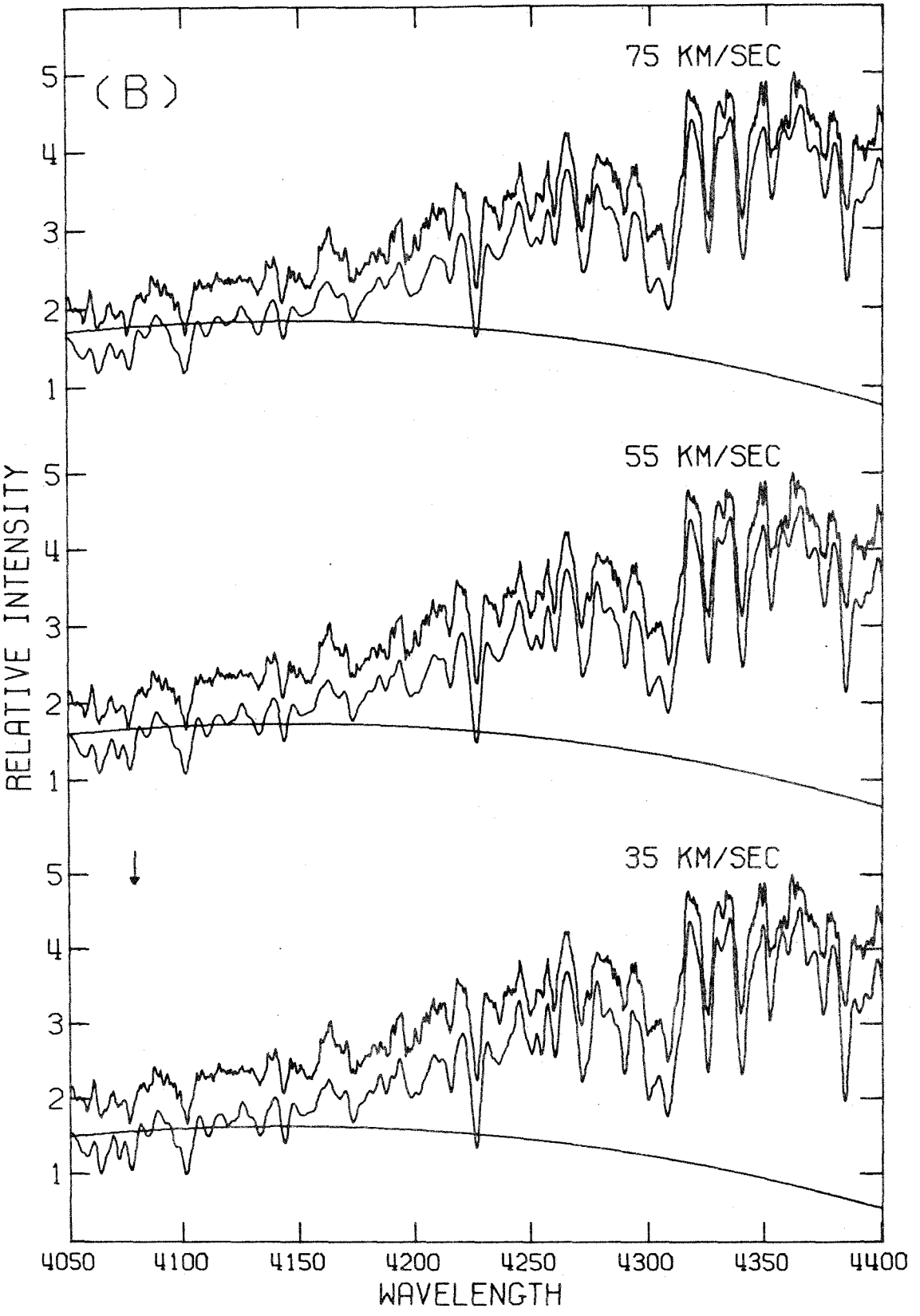
(B)
75 KM/SEC
55 KM/SEC
35 KM/SEC
RELATIVE INTENSITY
1
2
3
4
5
4050
4100
4150
4200
4250
4300
4350
4400
WAVELENGTH

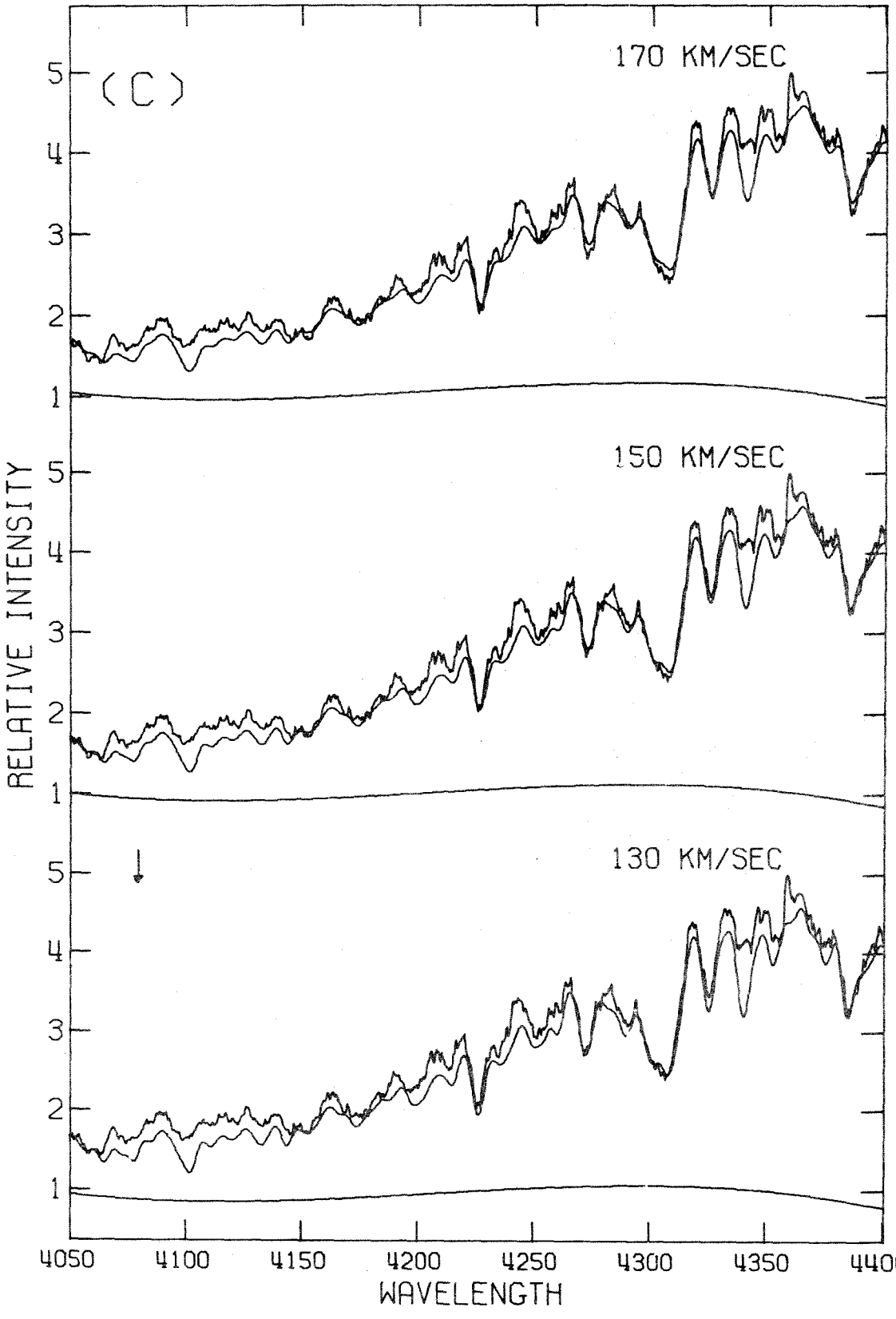
(C)
170 KM/SEC
150 KM/SEC
130 KM/SEC
RELATIVE INTENSITY
WAVELENGTH
1
2
3
4
5
4050
4100
4150
4200
4250
4300
4350
4400

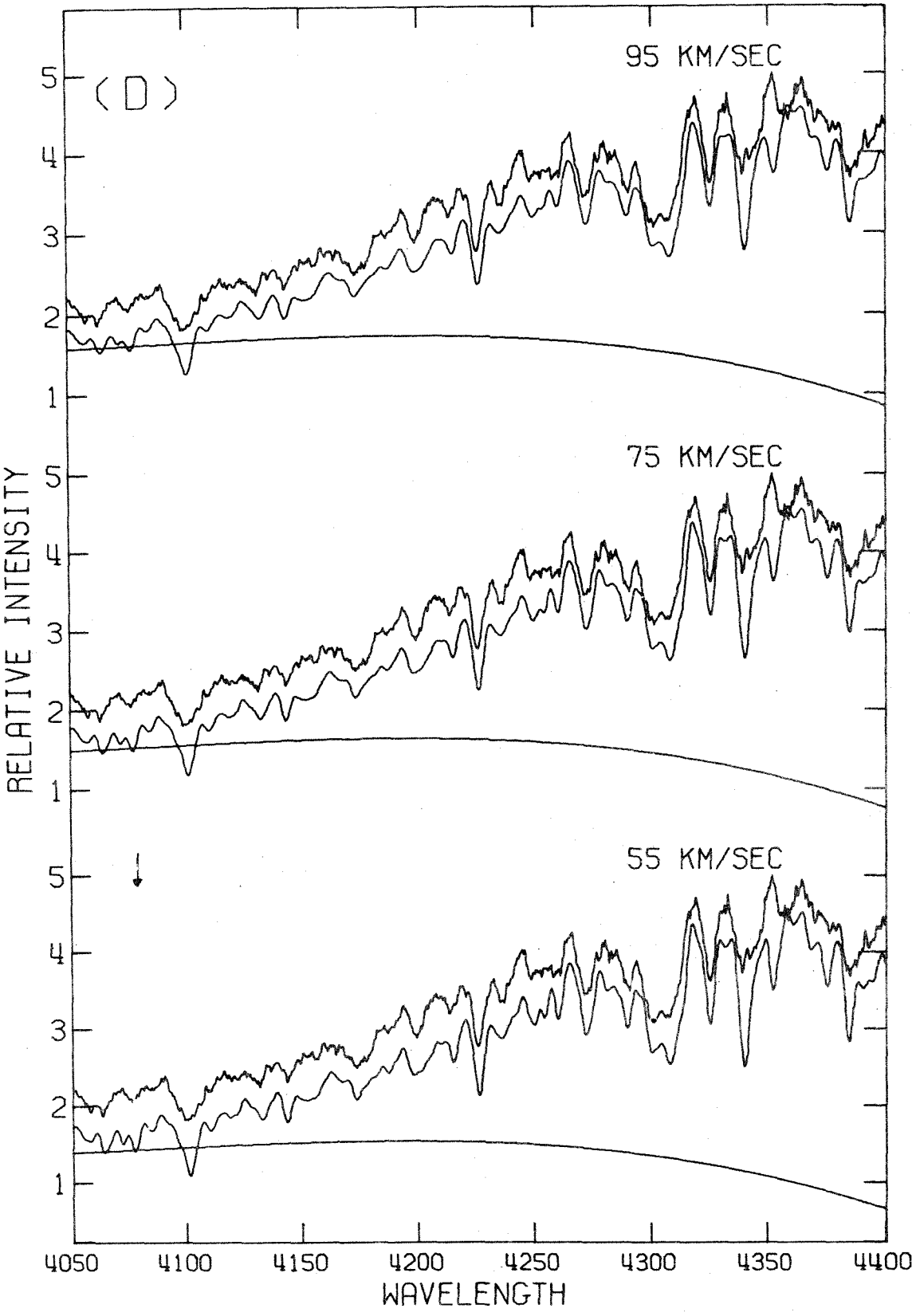
(D)
95 KM/SEC
75 KM/SEC
55 KM/SEC
RELATIVE INTENSITY
WAVELENGTH
4050
4100
4150
4200
4250
4300
4350
4400
1
2
3
4
5

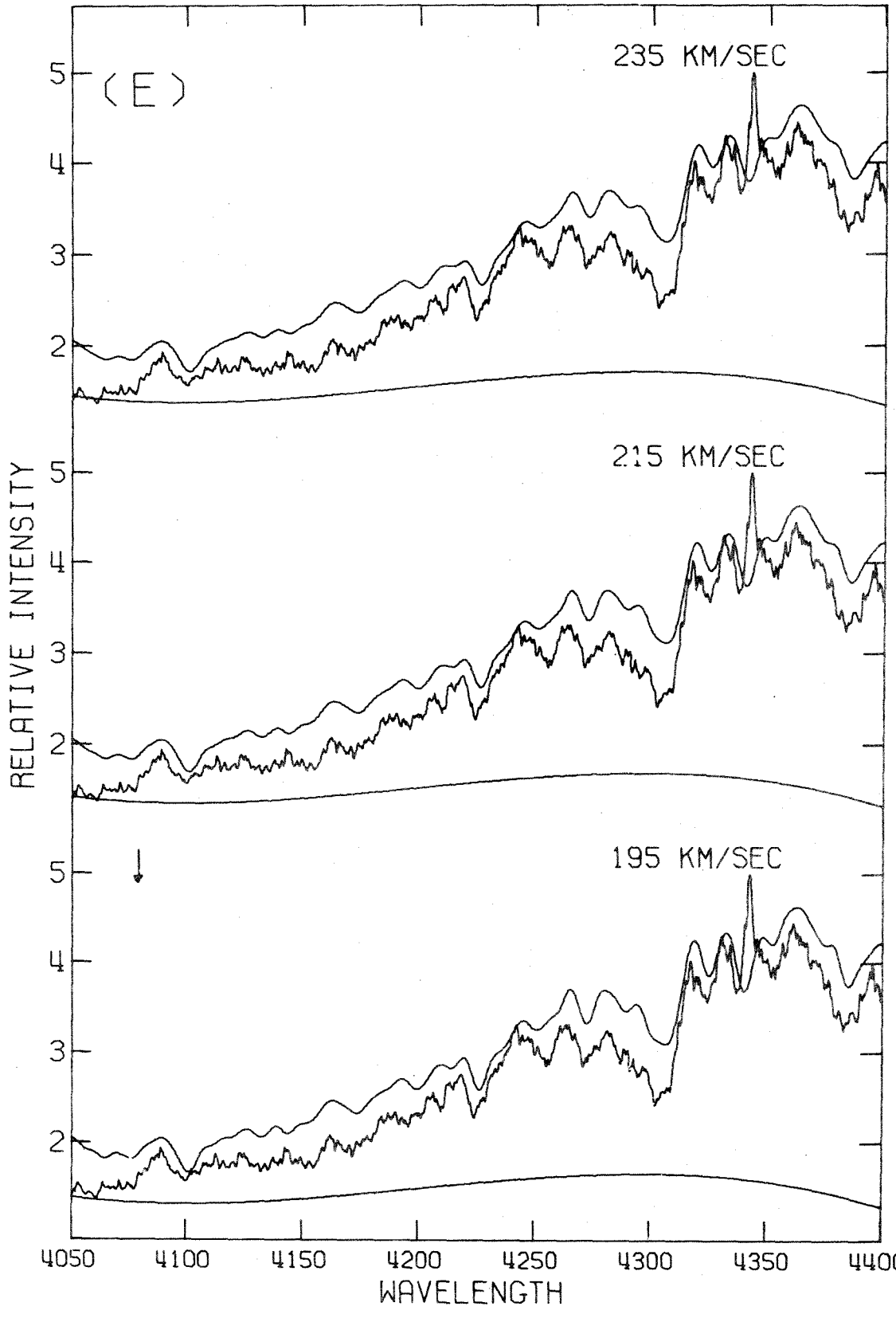
(E)
235 KM/SEC
215 KM/SEC
195 KM/SEC
RELATIVE INTENSITY
WAVELENGTH
2
3
4
5
4050
4100
4150
4200
4250
4300
4350
4400

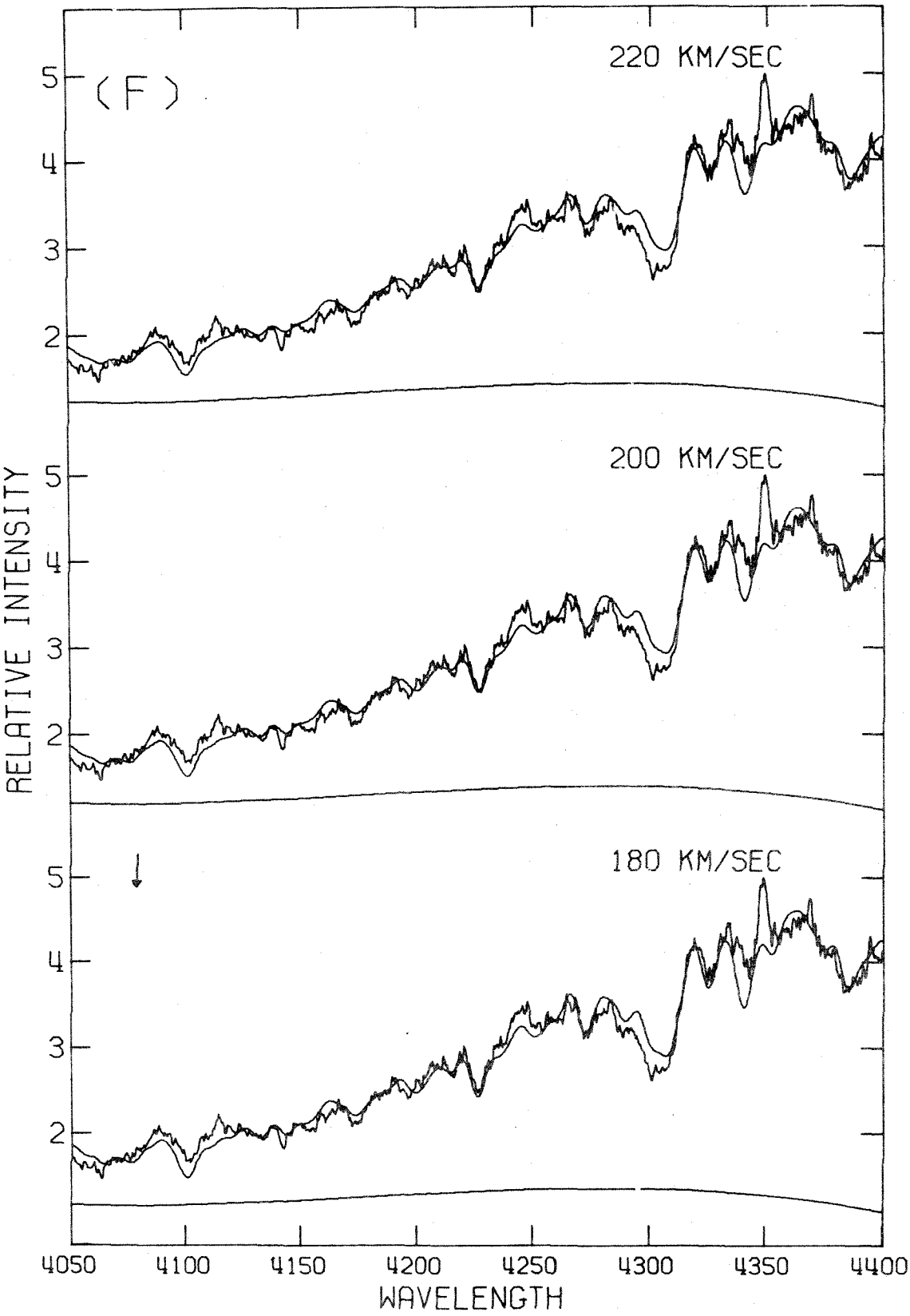
(F)
220 KM/SEC
200 KM/SEC
180 KM/SEC
RELATIVE INTENSITY
WAVELENGTH
2
3
4
5
4050
4100
4150
4200
4250
4300
4350
4400

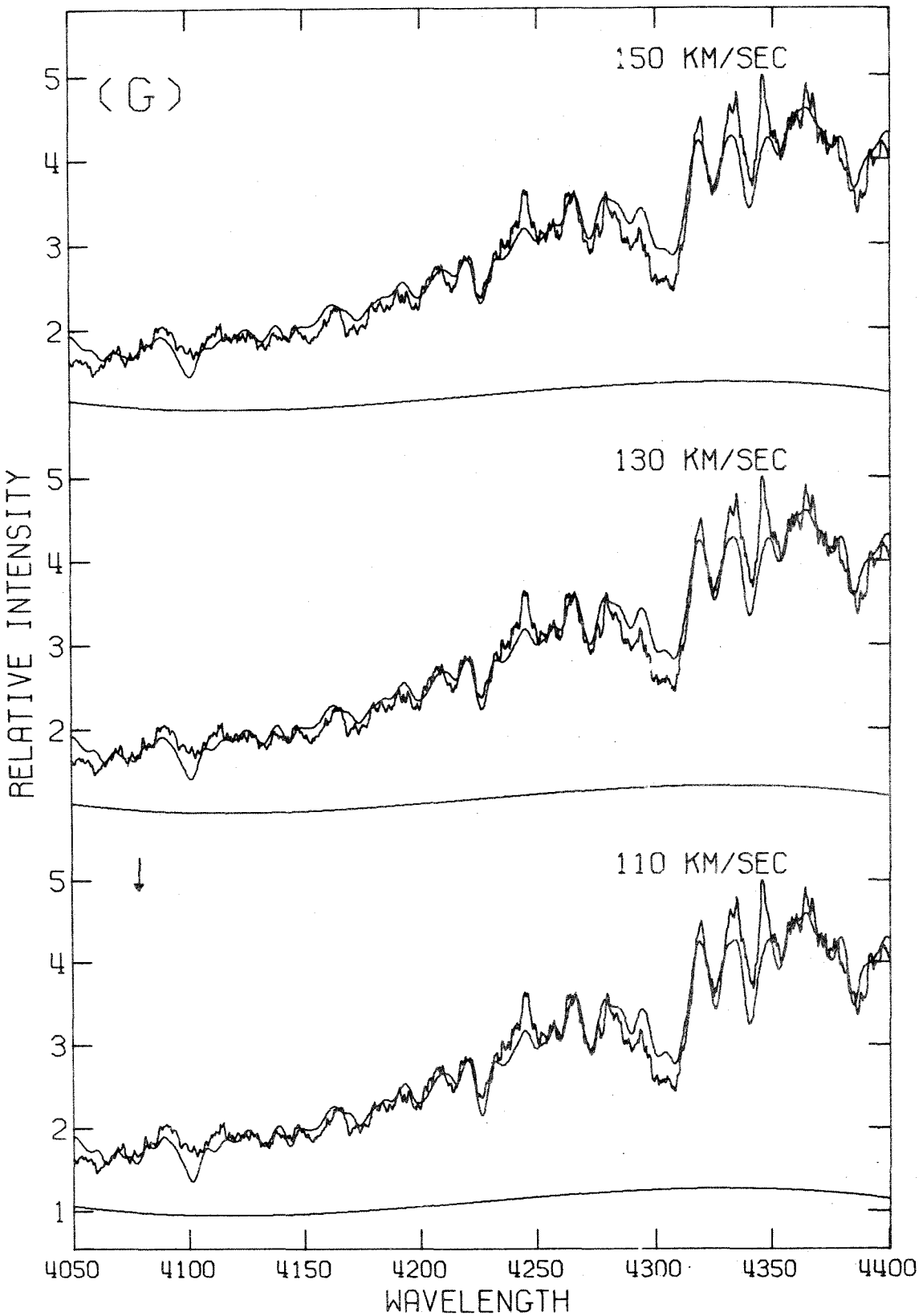
(G)
150 KM/SEC
130 KM/SEC
110 KM/SEC
RELATIVE INTENSITY
WAVELENGTH
4050
4100
4150
4200
4250
4300
4350
4400

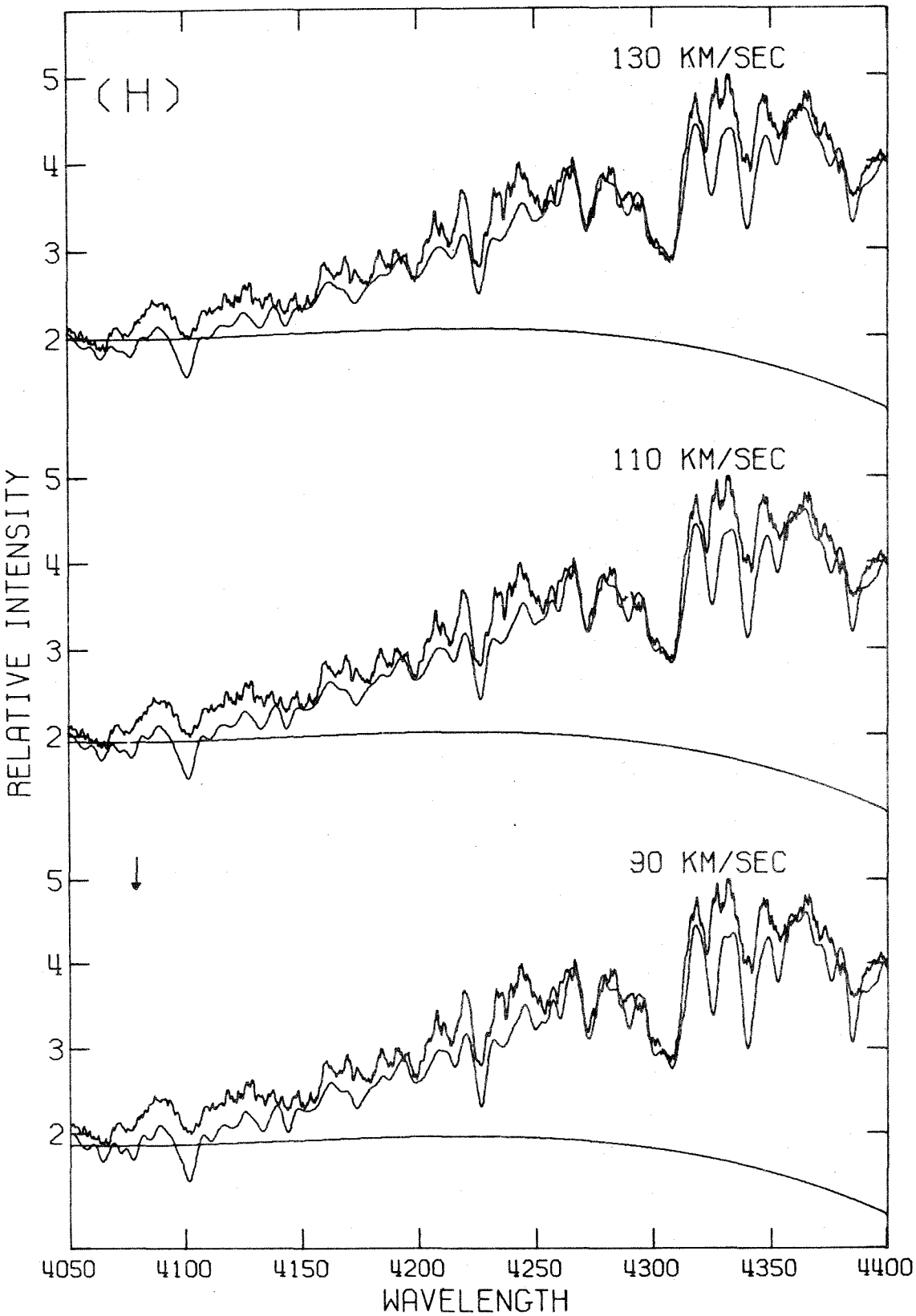
(H)
130 KM/SEC
110 KM/SEC
90 KM/SEC
RELATIVE INTENSITY
WAVELENGTH
2
3
4
5
4050
4100
4150
4200
4250
4300
4350
4400

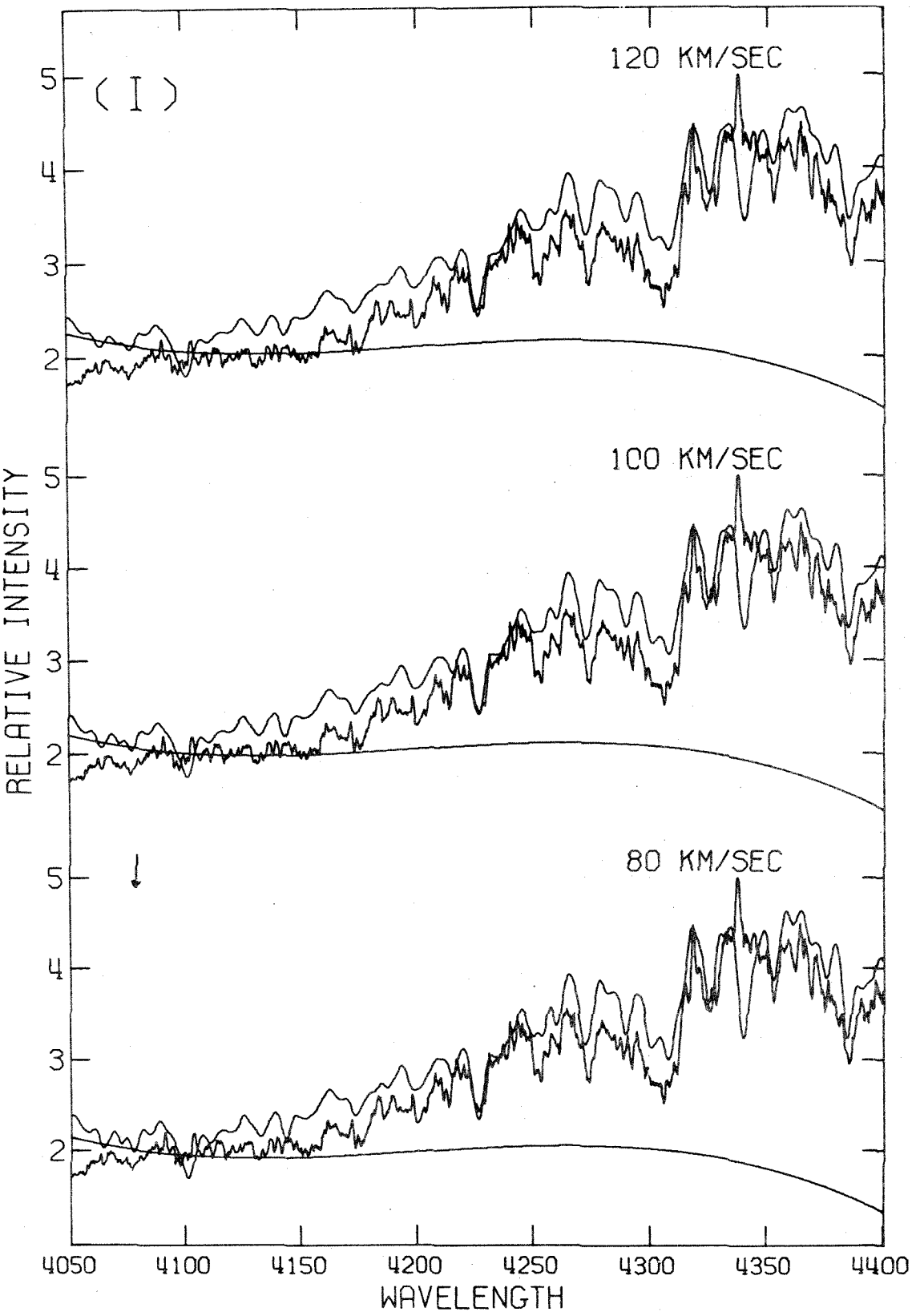
120 KM/SEC
(I)
100 KM/SEC
80 KM/SEC
RELATIVE INTENSITY
WAVELENGTH
5
4
3
2
4050
4100
4150
4200
4250
4300
4350
4400

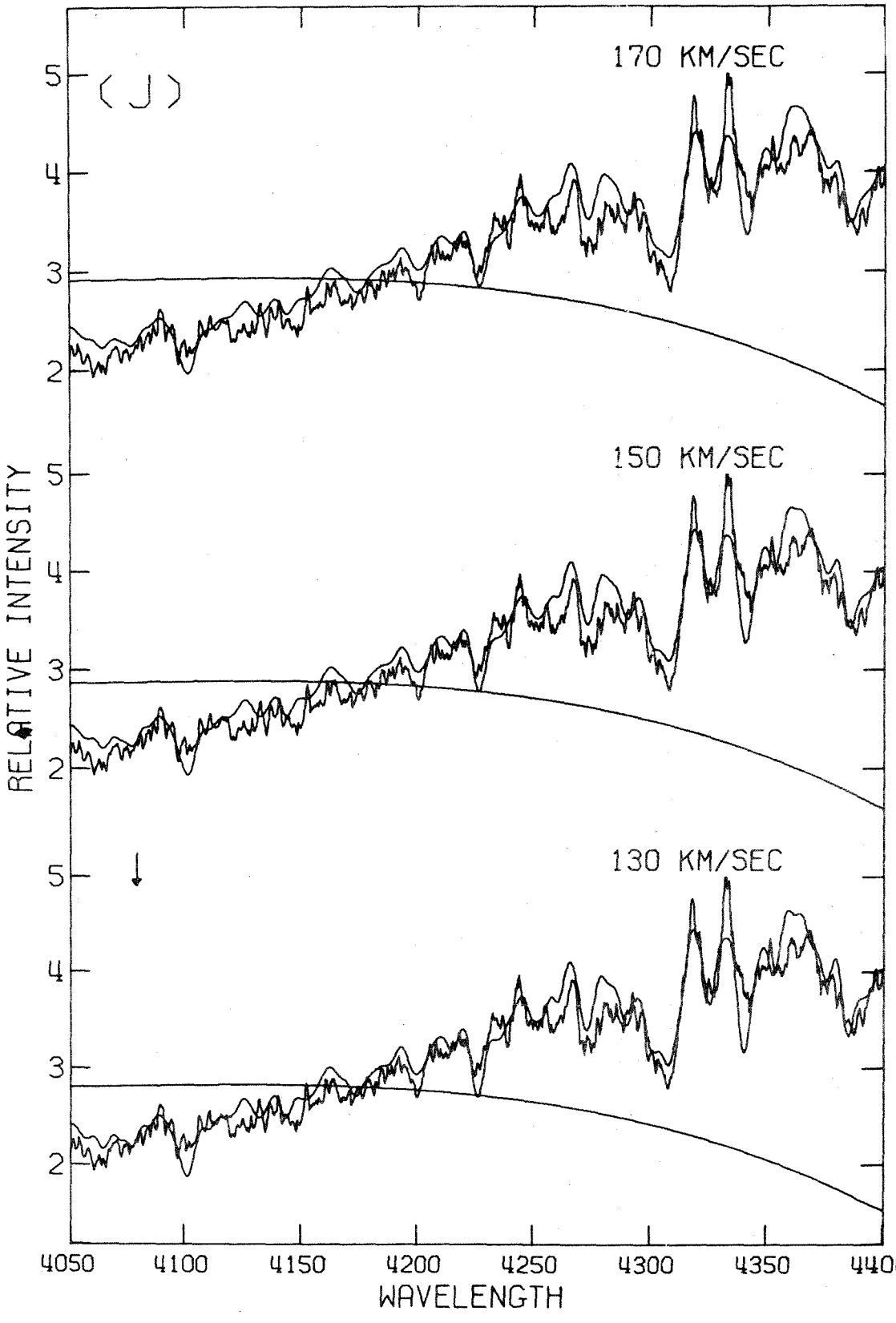
170 KM/SEC
(J)
150 KM/SEC
130 KM/SEC
RELATIVE INTENSITY
WAVELENGTH
2
3
4
5
4050
4100
4150
4200
4250
4300
4350
4400

than the values found by other authors and listed in Table 1 (excluding Minkowski's measurements, which are known to be too high). This discrepancy is much larger than the errors in wavelength registration between the spectra. The wavelength scales are accurate in this spectral region to 0.15 Å, and the sample size is 0.25 Å. We thus expect that the spurious broadening due to shifts in wavelength scale is less than 15 km sec^{-1}. To investigate this effect, spectra of single stars of spectral type late G III and early K III were broadened using the method described above and were compared with four of the galaxy spectra. These results are also listed in Table 1 and shown in Figure 2. These estimates agree with those previously derived by other authors using single stars to within 10 ± 10 km sec^{-1}. This good agreement suggests that it is the use of composite spectra which causes the above discrepancy, and not any systematic errors in the data reduction or in the visual comparison of observed and broadened spectra. This discrepancy is plausible. The composite spectrum, made up stars with different spectral types, will be more highly blended than the spectrum of any single star, and hence somewhat "broadened" even at zero velocity dispersion. For example, in early G stars the blue edge of the G band is stronger than the red edge; for early K stars, the reverse is true. Hence a composite

Figure 2

Velocity dispersion estimated from a single stellar spectrum. The upper curve of each pair is the broadened spectrum of a K0 III star; the lower is the observed spectrum of NGC 3379. The two spectra of each pair are separated a distance shown by the arrow. The smooth curve is a polynomial added to the stellar spectrum to adjust its color to that of the galaxy; this curve is drawn to the same relative intensity scale as the spectra, but with a zero point shift - zero is the level at 4200 Å. The best velocity dispersion is shown in the central plot.

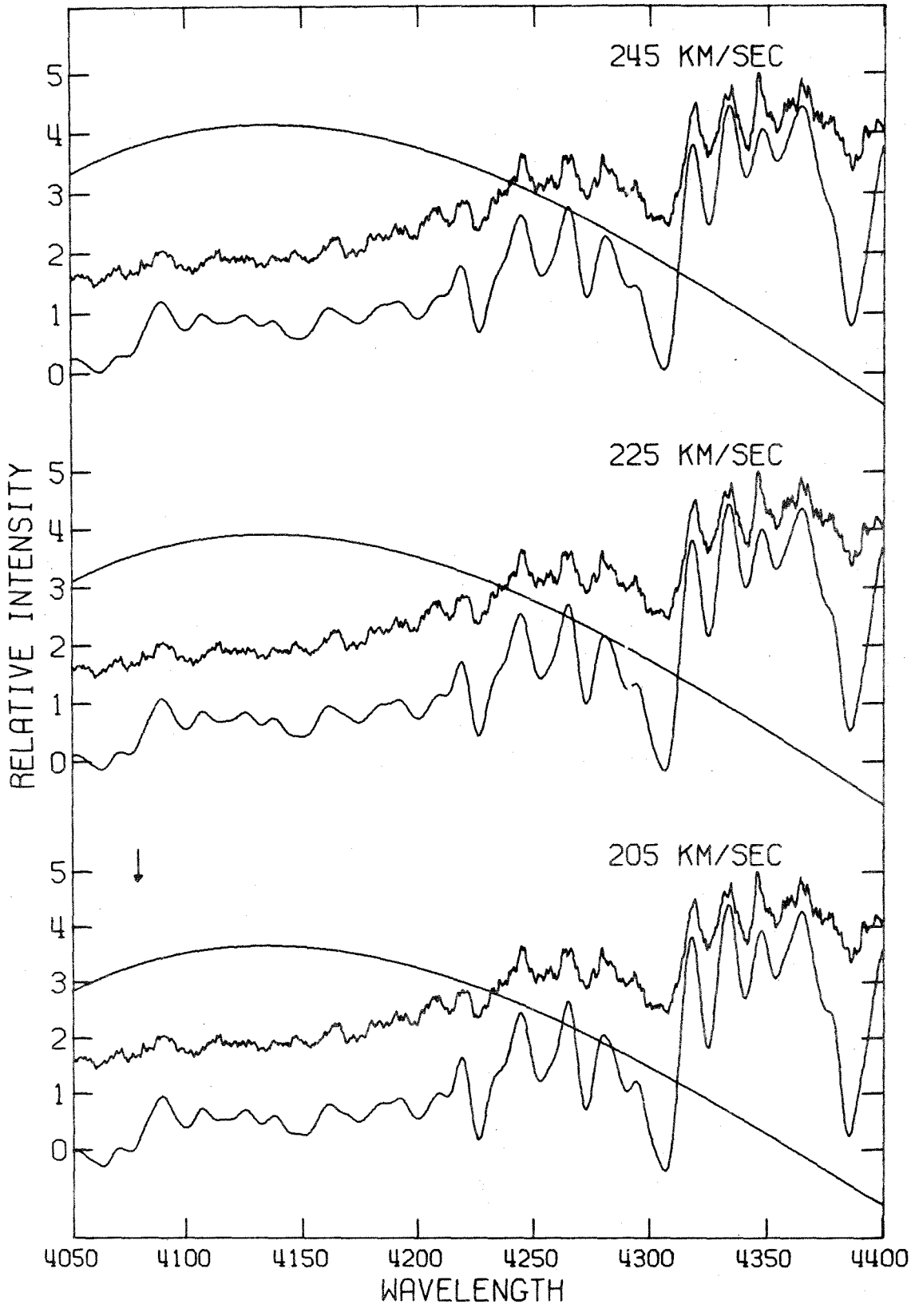
245 KM/SEC
225 KM/SEC
205 KM/SEC
RELATIVE INTENSITY
0
1
2
3
4
5
4050
4100
4150
4200
4250
4300
4350
4400
WAVELENGTH

spectrum made of both types of stars will have a more symmetric, "broadened" G band. Such discrepancies have also been mentioned by de Vaucouleurs (1974) as a possible source of error in previous work. Since a composite spectrum with line strengths approximately equal to those in the observed galaxy is the proper spectrum to be used in determining velocity dispersions, we feel that previous work on this subject has yielded velocity dispersions which are systematically too large. To determine an accurate velocity dispersion, a composite synthesized spectrum must be used.

IV. MASS TO LIGHT RATIOS

Using the velocity dispersions presented above, surface photometery of the galaxies, and assumptions about dynamic equilibrium, mass to light ratios may be derived for these galaxies. For the ellipticals, we use the relation derived from the virial theorem by Morton and Chevalier (1972):

$$\frac{M}{M_\odot} = 200\, \sigma^2\, \beta_{1/2}\, \left(\frac{a}{b}\right)^{2/3}\, v\, \left(\frac{50}{H}\right)$$

Where the velocity dispersion σ and recessional velocity v are in km sec^{-1}, the half-light radius $\beta_{1/2}$ is in arc seconds, the Hubble constant H is in km sec^{-1} Mpc^{-1}, and a/b is the axial ratio of the galaxy. The data for the

ellipticals are presented in Table 2; the photometric data for NGC 4473 and NGC 3379 are from Fish (1964), for NGC 3115 from van Houten (1961) and Morton and Chevalier (1973), for NGC 584 and 1052 from de Vaucouleurs (1964), with appropriate scaling, and for NGC 221 from Richstone and Sargent (1972). With the exception of NGC 221, the distances are estimated from the recession velocities, using a Hubble constant of 50 km sec^{-1} Mpc^{-1}; for the nearer galaxies these estimates may have large relative error due to the peculiar velocities of the galaxies. The mass to light ratios presented in Table 2 are for the photographic band. If the errors in the photometery are 10%, in the velocity dispersions 15%, and in the distances 20%, then the errors in M/L are 37%. Since the simple application of the virial theorem which leads to the above formula is undoubtedly an oversimplification of the actual physical situation, the true errors in these estimates of the mass to light ratio may be much larger, but arise from theoretical rather than observational errors.

For the spirals, the above formula is inadequate, since the observed velocity dispersions arise from the spheroidal component of a more complicated bulge-disk system. Spinrad, et al. (1971) present a formula for the mass to light ratio of the core region which is insensitive to the structure of the outer regions:

TABLE 2

MASS TO LIGHT RATIOS FOR ELLIPTICALS

Galaxy (NGC)	Type	Distance† (Mpc)	b/a	$\beta_{1/2}$ (arc sec)	σ (km sec^{-1})	Mass† ($10^{11} M_\odot$)	m_{pg} (mag)	L† ($10^{10} L_\odot$)	M/L†* ($M_\odot/L_\odot$)
3379	E1	14.9 h^{-1}	0.88	44.5	133	1.3 h^{-1}	10.8	1.5 h^{-2}	8.7 h
221	E2	0.69 h^{-1}	0.80	51.3	55	0.012 h^{-1}	9.06	0.016 h^{-2}	7.5
584	E4	37.7 h^{-1}	0.60	23.0	150	2.7 h^{-1}	11.6	4.6 h^{-2}	5.9 h
1052	E4	28.9 h^{-1}	0.50	14.9	100	0.68 h^{-1}	11.6	2.7 h^{-2}	2.5 h
4473	E5	43.4 h^{-1}	0.60	19.7	110	1.5 h^{-1}	11.3	8.0 h^{-2}	1.9 h
3115	E7-SO	9.4 h^{-1}	0.47	44.0	200	2.7 h^{-1}	10.1	1.1 h^{-2}	25.0 h

† h= 50 Ho^{-1}

* in photographic band

$$\frac{M}{L} = \frac{C \ <\sigma^2>}{I_o \ \theta_c \ R}$$

where: $C = 0.19 \ (\ 0.3 + 0.7 \ \frac{b}{a} \ )^{-1}$

Here I_o is the central surface brightness, θ_c is the core radius, defined as the point where $I = 1/2 \ I_o$, R is the distance to the galaxy, and σ is the observed velocity dispersion. With R in Mpc, θ_c in arc seconds, I_o in terms of equivalent 20^{th} magnitude stars per square arc second, and σ in km sec^{-1}, M/L is in solar units. Using this formula, mass to light ratios are derived for the central components of the spiral galaxies observed. The data are presented in Table 3. The photometry for NGC 224 is from Light, et al.(1974), for NGC 3031 from Brandt, et al. (1972) and Goad (1974), for NGC 4594 from van Houten (1961), and for NGC 5194 from Schweitzer (private communication). The mass to light ratios are for the V band for all except NGC 4594, which is for the photographic band. The above comments about the magnitude of the errors for the ellipticals are equally applicable here. Using standard colors for the spirals estimated from de Vaucouleurs (1964), the M/L ratios in V light may be multiplied by a factor 3.1 to convert them to the photographic band, for comparison with the ellipticals.

TABLE 3

MASS TO LIGHT RATIOS FOR SPIRALS

Galaxy (NGC)	Type	Distance† (Mpc)	b/a	θ_c (arc sec)	I_o† (eq.stars)	σ (km sec^{-1})	M/L†* ($M_\odot/L_\odot$)
4594	Sa	20.0 h^{-1}	0.50	1.0	54 h^{-2}	215	12.6 h
224	Sb	0.69	0.63	0.56	832	125	12.5
3031	Sb	3.0 h^{-1}	0.85	4.2	69 h^{-2}	150	5.5 h
5194	Sc	11.0 h^{-1}	0.95	2.9	28 h^{-2}	75	1.2 h

† $h = 50\ H_o^{-1}$

* 224, 3031, 5194 in V band; 4594 in photographic band

V. SUMMARY

The use of single stellar spectra in previous works to estimate velocity dispersions has led to results which were systematically too large. We believe that the estimates presented in this paper, based upon composite spectra very similar to the galaxy spectra, are better measurements of the actual velocity dispersions in these galaxies. This result implies that future attempts to estimate velocity dispersions must include a study of the stellar population and the construction of the appropriate composite spectrum for the galaxy.

The mass to light ratios presented in Tables 2 and 3 are small, reflecting the lower estimates of the velocity dispersions. These results thus exacerbate the problem of the "missing mass". Moreover, these low M/L values for the centers of galaxies rule out such exotic explanations as "black holes in the nuclei of galaxies". A new study by Turner (1975) of binary galaxies finds mass to light ratios which are five times larger than those estimated in this paper. To resolve these discrepancies, one must speculate that the M/L ratio increases dramatically towards the outer parts of galaxies.

There seems to be no systematic difference between the mass to light ratios for spirals and ellipticals. Thus the inner part of the bulge component of spiral

galaxies appears to be similar to the material in elliptical galaxies.

The mass to light ratios for two of these galaxies are in good agreement with those derived from the population syntheses of Paper I. The rest seem to be approximately a factor of two lower than those in Paper I. In view of the large inaccuracies of the mass to light estimates derived from population synthesis, and the uncertainties of the theoretical treatment given above, these discrepancies are not disturbing. The population syntheses have probably included too many late M dwarfs, which rapidly increase the M/L ratio. Reducing the M dwarf fraction in the models of Paper I would not affect any of the results of this paper, since these stars contribute little to the light of the composite spectra.

The author wishes to thank Dr. F. Schweitzer for kindly providing the surface photometry data for NGC 5194 in advance of publication. Drs. D. Richstone and T. Thuan provided helpful advice during the course of this work. The author was supported during part of this work by a National Science Foundation pre-doctoral fellowship. I would like to especially thank J. Hoessel for his assistance on this project.

REFERENCES

Brandt, J. C., Kalinowski, J. K., and Roosen, R. G. 1972, Ap. J. Suppl., 210, 421.

Burbidge, E. M., Burbidge, R. R., and Fish R. A. 1961a, Ap. J., 133, 393 and 1092 (correction).

_____ 1961b, Ap. J., 134, 251.

de Vaucouleurs, G. 1974 in I.A.U. Symposium No. 58, ed. J. R. Shakeshaft (Dordrecht: Reidel), p. 1.

de Vaucouleurs, G., and de Vaucouleurs, A. 1964, Reference Catalogue of Bright Galaxies (Austin: University of Texas Press).

Faber, S. M., and Jackson, R. E. 1975, preprint.

Fish, R. A. 1964, Ap. J., 139, 284.

Goad, J. W. 1974, Ap. J., 192, 311.

Minkowski, R. 1962, in I.A.U. Symposium No. 15, ed. G. McVittie (New York: MacMillan), p. 112.

Light, E. S., Danielson, R. E., and Schwarzschild, M. 1974, Ap. J., 194, 257.

Morton, D. C., and Chevalier, R. 1972, Ap. J., 174, 489.

_____ 1973, Ap. J., 179, 55.

Morton, D. C., and Thuan, T. X. 1973, Ap. J., 180, 705.

Richstone, D., and Sargent, W. L. W. 1972, Ap. J., 176, 91.

Schweitzer, F. 1975, private communication.

Spinrad, H., Sargent, W. L. W., Oke, J. B., Neugebauer, G., Landau, R., King, I. R., Gunn, J. E., Garmire, G., and Dieter, N. H. 1971, Ap. J. (Letters), 163, L25.

Turner, E. L. 1975, Ph.D. Thesis, California Institute of Technology.

van Houten, C. J. 1961, Bull. Astr. Inst. Netherlands, 16, 1.

Williams, T. B. 1976, Ap. J., in publication.